INSTITUTE FOR DIRECT ENERGY CONVERSION

TOWNE SCHOOL

UNIVERSITY OF PENNSYLVANIA

PHILADELPHIA, PENNSYLVANIA

MANFRED ALTMAN, DIRECTOR

STATUS REPORT

INDEC-SR-11

NATIONAL AERONAUTICS AND SPACE ADMINISTRATION

GRANT NSG - 316

March 1967

1. MATERIALS ENGINEERING

Branch Chief: Dr. Solomon Pollack

Senior Members: Dr. Manfred Altman, Dr. Louis Girifalco,

Dr. Ram Sharma

TABLE OF CONTENTS

1.1 High Temperature Thermal Diffusivity Measurement

Senior Investigators: Dr. Manfred Altman, Dr. Ram Sharma

Ph.D. Student: K. Sreenivasan

Objectives

To develop an exper imental technique suitable for the determination of thermal diffusivities at high temperatures, primarily for the testing of thermal energy storage materials in the liquid state.

Previous Accomplishments

Phase 1: The theory of transient technique was studied and a new technique applicable to liquids was developed.

Phase 2: The furnace and measuring equipment were designed and built.

Progress in Past Period

The thermal diffusivity of the container material was measured. The liquid diffusivity cell was calibrated with a liquid whose thermal diffusivity is known. Thermal diffusivity of liquid Lithium Fluoride was measured. Details are presented on page A1-1.

1.1 Thermal Diffusivity

R. A. Sharma H. Keramaty

Thermal diffusivity of the mixtures of Calcium Fluoride and Barium Fluoride with compositions 33.3% CaF_2 and 66.7% CaF_2 (balance BaF_2) have been measured.

The thermal diffusivity variation with temperature and composition is shown in Table I and Fig. I.

Further work on the measurements of different materials and mixtures is in progress to establish some relationship between diffusivity of the mixtures and their components. See page A1-6 and A1-7.

A paper on "Thermodynamic Study of Mg-Ge System" was presented at A.S.M.E. Exposition & Congress in November, 1966, in New York.

1.2 Experimental Determination of the Thermoelectric Properties of Graphite Alloys

Senior Investigator: Dr. S. R. Pollack

Graduate Student: J. J. Curry

Objectives

The objective of this experiment is to develop new high efficiency thermoelectric energy conversion materials.

Previous Accomplishments

Experimental apparatus has been assembled that will enable measurements of the thermoelectric power, electrical conductivity, and Hall coefficient over a temperature range of $77^{\circ}K$ to $350^{\circ}K$.

Progress in Past Period

Several semiconductor compounds were fabricated and studied. Large thermoelectric powers ($\geq 340 \mu v/^{\circ}C$) were realized. Fabrication techniques are being investigated. For details see page A1-8.

1.3 Tunnel Emission Cold Cathodes

Senior Investigator: Dr. S. R. Pollack

Graduate Student: S. Basavaiah

Objectives

The purpose of this investigation is to develop efficient cold cathodes for electric devices, and, eventually to the development of tunnel emission devices and the study of hot electron transport phenomena. The by-products of this work are expected to be a better understanding of the electron scattering mechanisms in thin films with applicability to thin film solar cells and similar devices.

Previous Accomplishments

A new vacuum system design was completed after many futile attempts to utilize the Elion system.

Progress in Past Period

The new system was completed and tested, and successfully used to fabricate W-W_xO_y-Au samples. The preliminary results of the current-voltage characteristics are being studied. For details see page A1-10.

1.4 Studies of Thermal Transpiration for the Development of a Thermal Pump

Dr. M. Altman Mr. E. Hopfinger

Objectives

To develop a gas pump without moving parts based on the thermal transpiration principle.

Previous Accomplishments

Theoretical analyses of idealized system.

Progress in Past Period

The apparatus has been assembled and preliminary experimental results were obtained using Helium. These data show the general characteristics of such a pump. Details on page A1-13.

2. PLASMA ENGINEERING

Branch Chief: Leon W. Zelby

Senior Members: Michael Kaplit, George Schrenk, Samuel Schweitzer, Hsuan Yeh

2.1 Slow Wave Plasma Diagnostics

W. H. Becker L. W. Zelby

Objectives

To develop slow wave plasma interaction for measurement of local plasma parameters.

Progress in Past Period

Experimental equipment was re-assembled for measurements on plasma columns of different radii (from 1.0 to 3.0 cm.). Measurements of plasma decay time as functions of initial plasma current and gas pressure were made indicating a possibility of electron temperature, and mean free path determination. Figures are shown on page A2-1 and A2-2.

2.2 Plasma Centrifuge

M. Altman S. Schweitzer
P. Hsueh

Objectives

To evaluate obtainable velocities in a plasma spinning in the annular space between two concentric cylinders under the influence of a longitudinal magnetic field and a radial electric field.

Previous Accomplishments

First phase completed.

Progress in Past Period

Mr. Peter Hsueh has submitted his thesis. This work has resulted in a new project entitled "Flow of a Conducting Liquid in an Annular Gap" which follows.

2.3 The Flow of a Conducting Liquid in an Annular Gap

S. Schweitzer I. M. Cohen*

Objectives

To study the flow field, current distribution, and magnetic field in an annular gap filled with a conducting fluid and driven electromagnetically.

Previous Accomplishments

Theoretical Analysis for the case of liquid mercury was completed (for details see INDEC SR-8).

Progress in Past Period

One dimensional, inviscid flow of mercury in an annular gap, driven electromagnetically has been studied. For details see page A2-3.

---

* Assistant Professor of Mechanical Engineering, Towne School of Civil and Mechanical Engineering, University of Pennsylvania.

2.4 Experimental Study of an Electromagnetically Driven Mercury Centrifuge

S. Schweitzer I. M Cohen*

T. Ebtekar

Objectives

To study the operation parameters of a mercury centrifuge.

Previous Accomplishments

None

Progress in Past Period

Design of a simple mercury centrifuge, driven electromagnetically has been completed. Provisions for measurements of velocity and pressure distributions as well as skin friction coefficients have been made. Apparatus is under construction.

---

* Assistant Professor of Mechanical Engineering, Towne School of Civil and Mechanical Engineering, University of Pennsylvania.

2.5 The Influence of High Fields on Surface Charge Distributions

G. L. Schrenk S. Fonash

Objectives

To determine the effect of high fields on the work function of metals.

Previous Accomplishments

Emphasis is being placed on the problem of understanding the varying average intensity of the different regions of field ion micrographs. These regions are sharply defined and are more pronounced in some metals than in others. (For example, in platinum they form one of the most prominent features of the micrograph, while in tungsten they are barely discernible.)

The explanation of these sharply defined regions appears to be related to the band structure of metals at their Fermi levels. We only need to consider the Fermi level because, at the low temperature and high field strengths involved, tunneling occurs only to the Fermi level of the metal.

Progress in Past Period

Current research is focused on the construction of a quantum mechanical model of this tunneling process. This research is further complicated by the lack of knowledge of the Fermi surfaces of the metals involved; thus considerable efforts are also being devoted to investigating the Fermi surfaces involved. Results will be made available in future reports.

2.6 Anistropy of Metal Work Functions

M. Kaplit

Objective

To develop a model accounting for different results of measurements of the work function of tungsten.

Previous Accomplishments

Effects of surface stresses and polarizabilities were calculated.

Progress in Past Period

Study completed with the calculation of the work function differences between the four planes of tungsten; (110), (211), (100), (111).
For details see page A2-10.

2.7 Characteristics of Thermionic Plasma Diodes with Gas Mixtures

G. L. Schrenk A. Kaufman

Objectives

To develop a quantitative model for "seeded" diodes for the purpose of evaluating the Penning effect.

Previous Accomplishments

The mathematical models for both the ignited and the unignited modes of a plasma diode using a gas mixture have been completed.

Progress in Past Period

The results of these models are currently being studied. For details see page A2-20.

3. ELECTROCHEMICAL ENGINEERING

Branch Chief: Dr. Leonard Nanis

Senior Member: Dr. John O' M. Bockris

Postdoctoral Research Associate: Dr. Philippe Javet

3.1 The Design of Absorption Towers Dissolving H_2 and O_2 in Aqueous KOH

Senior Investigator: Dr. L. Nanis

Graduate Student: Mr. Irving Klein

Objectives

This is a special project undertaken at the suggestion of NASA to determine, using conventional chemical engineering methods, the feasibility of a fuel cell system which does not rely on porous electrodes. Fuel gas is dissolved into electrolyte in contact towers and is reacted between flat electrodes. Spent electrolyte is recycled through the towers.

Previous Accomplishments

New project.

Progress in Past Period

Contact towers for saturating H_2 and O_2 into 4N KOH were designed. Tower heights of about 5 feet were computed for 1 square foot cross section. Crude estimates of pumping losses indicate about one-fourth of the output of a 200 watt fuel cell would be consumed in a parasitic mode. Future work will deal with improved loss calculations for towers and cell stacks as well as total size considerations.

For further details, see Appendix A3-1.

3.2 Overpotential - Time Variation for Galvanostatic Charging with Potential Dependent Capacitance

Senior Investigator: Dr. L. Nanis
Research Associate: Dr. P. Javet

Objectives

The goal of this effort is essentially stated in Sec. 3.3 namely the development of simplified mathematics for electrochemical engineering.

Previous Accomplishments

A modification to the full rate equation (overpotential vs. current density) was found to permit solution of the non-linear equation for overpotential vs. time.

Progress in Past Period

As indicated in SR-9, the effect of a linear potential dependent capacity has been investigated. A considerable distortion of η vs. t occurs in comparison with the case of constant capacity.

For details see Appendix A3-28.

3.3 Current and Potential Distribution in Cylindrical Geometries: Engineering Applications to Fuel Cell Design

Senior Investigator: Dr. L. Nanis

Objectives

The purpose of these efforts is to develop simplified treatments of the mathematics which underlie fuel cell design and behavior. For engineering purposes, the compact notation favored by mathematicians is elegant but not useful. Attention will be devoted to simplifying the mathematics wherever possible and indicating design parameters which evolve in considerations of potential and current distribution in porous electrode models and related heat and mass transfer computations.

Previous Accomplishments

New Project

Progress in Past Period

Fourier - Bessel transforms have been used to generate a useful result in matrix cell design. The resistance due to screen contacts on a matrix sandwich has been evaluated for the limits of constant potential and constant current density.

For details see Appendix A3-32.

3.4 Foaming Electrolyte Fuel Cell

Senior Investigator: Dr. L. Nanis

Research Specialist: Mr. A. Saunders

Objectives

This work derives from considerations of diffusion as an ultimate fuel cell limitation step and methods to avoid the use of porous electrodes. Rapid gas saturation into electrolyte can be accomplished by providing large contact area and short diffusion path. Electrolyte foam is theoretically ideal for this purpose and laboratory studies are needed to verify this approach.

Previous Accomplishments

New project.

Progress in Past Period

Remarkable improvement over bulk electrolyte behavior is obtained for electrodes operating through electrolyte foam, despite higher resistance. Feasibility of this method is being extended to improved cell design. For details see Appendix A3-41.

4. PUBLICATIONS LIST

Publications List

INDEC-1 "The Optimization of MHD Generators with Arbitrary Conductivity", H. Yeh and T. K. Chu, ASME Paper 63-WA-349.

INDEC-2 "The Prediction of Transient Heat Transfer Performance of Thermal Energy Storage Devices", M. Altman, D. P. Ross, H. Chang, Proceedings of 6th National Heat Transfer Conference, Boston, Mass., 1963.

INDEC-3 "The Binary Eutectic as a Thermal Energy Storage System: Equilibrium Properties", G. R. Belton and Y. K. Rao, paper presented at the 6th National Heat Transfer Conference, Boston, Mass., Aug. 11-14, 1963.

INDEC-4 "Theoretical Model of a Thermionic Converter", J. Dunlop and G. Schrenk, Proceedings of Thermionic Specialist Conference, Gatlinburg, Tenn., pp. 57-62, Oct. 7-9, 1963.

INDEC-5 "Thermophysical and Transport Properties of High Temperature Energy Storage Materials", R. Sharma and H. Chang, paper presented at the Third Annual Symposium, High Temperature Conversion Heat to Electricity, Tucson, Arizona, Feb. 19-21, 1964.

INDEC-6 "Solar Collection Limitations for Dynamic Converters - Simulation of Solar-Thermal Energy Conversion Systems", G. L. Schrenk, Proceedings of AGARD Conference, Cannes, France, March 16-20, 1964.

INDEC-7 "Prospects for Thermal Energy Storage", M. Altman, Proceedings of AGARD Conference, Cannes, France, March 16-20, 1964.

INDEC-8 "The Hollow Thermionic Converter", L. Zelby, IEEE Annual Meeting on Energy Conversion, Clearwater, Florida, May, 1964.

INDEC-9 "The Institute for Direct Energy Conversion", M. Altman, paper presented at Am. Soc. Eng. Ed. Annual Meeting, University of Maine, Orono, Maine, June 22-26, 1964.

INDEC-10 "Emitter Sheath Polarity in Plasma Diodes", G. Schrenk, Proceedings of Thermionic Specialist Conference, Cleveland, Ohio, Oct. 26-28, 1964, pp. 249-257.

INDEC-11 "Electron Emission from Metals in Gaseous Environment", M. Kaplit, G. Schrenk, L. Zelby, Proceedings of Thermionic Specialist Conference, Cleveland, Ohio, Oct. 26-28, 1964, pp. 4-10.

INDEC-12 "Criteria for Emitter Sheath Polarity in Plasma Diodes", G. Schrenk, paper presented at ASME Winter Annual Meeting, New York, No. 29, Dec. 3, 1964.

INDEC-13 "An Electrochemical and Microbiological Study of the Formic Acid-Formic Dehydrogenlyase System", R. J. Blasco and E. Gileadi, Advanced Energy Conversion, Vol. 4, pp. 179-186, 1964.

INDEC-14 "Mathematical Simulation of Solar Thermionic Energy Conversion Systems", G. Schrenk and A. Lowi, Proceedings of the International Thermionic Electrical Power Generation Conference, IEEE, London, England, Sept. 20-24, 1965.

INDEC-15 "Cavity Receiver Temperature Analysis", R. McKinnon, A. Turrin, G. Schrenk, AIAA paper No. 65-470, July 26-29, 1965.

INDEC-16 "Electron Emission from Metals in Vapors of Cesium and Fluorine", G. Schrenk and M. Kaplit. Proceedings of the Thermionic Specialist Conference, San Diego, California, Oct. 25-27, 1965.

INDEC-17 "Longitudinal Interaction of Microwaves with an Argon Discharge", C. A. Renton and L. W. Zelby, Appl. Phys. Ltrs., Vol. 6, No. 8, pp. 167-169, Sept. 15, 1965.

INDEC-18 "Microwave Interaction with a Non-Uniform Argon Discharge", L. W. Zelby, Proceedings of the Symposium of Microwave Interaction with Ferrimagnetics and Plasmas, London, England, pp. 32-1 to 32-3, Sept. 13-17, 1965.

INDEC-19 "Two-Phase Flow and Heat Transfer for Boiling Liquid Nitrogen in Horizontal Tubes", M. Altman and J. H. Jones, Chemical Engineering Progress Symposium Series, Volume 61, No. 57, Oct. 1965.

INDEC-20 "Electrical Conductivity of a Partially Ionized Gas in a Magnetic Field", S. Schweitzer and M. Mitchner, Submitted to the AIAA Journal.

INDEC-21 "Models for Electron Emission from Metals with Adsorbed Monolayers", M. Kaplit and G. L. Schrenk, Submitted to Advanced Energy Conversion.

INDEC-22 "Models for Electron Emission from Metals with Adsorbed Monolayers", M. Kaplit and G. L. Schrenk, paper presented at Twenty-Sixth Annual Conference on Physical Electronics, Massachusetts Institute of Technology, Cambridge, Mass., March 21-23, 1966.

INDEC-23 "Slow Wave Interaction with an Argon Discharge", (Abstract) L. W. Zelby, Symposium on Properties and Applications of Low-Temperature Plasmas, XX-th International Congress of I.V.P.A.C., Moscow, USSR, July 15-18, 1965.

INDEC-24 "Understanding Plasma Diodes and Amplifiers", L. W. Zelby, Electronic Industries, Vol. 24, No. 11, p. 64, Nov. 1965.

INDEC-25 "A Simplified Approach to the Analysis of Electromagnetic Wave Propagation Characteristics of Plasma Coated Surfaces", L. W. Zelby, RCA Review, Vol. 26, No. 4, p. 497, Dec. 1965.

INDEC-26 "Plasma Coated Surface as a Wave Guide", L. W. Zelby, RCA Engineer, Vol. 11, No. 4, p. 50, Jan. 19, 1966.

INDEC-27 "Measurements of Collision Frequency in an Argon Discharge", L. W. Zelby, W. O. Mehuron, R. Kalagher, Applied Physics Letters, June 15, 1966, Vol. 21, No. 5, pp. 522-524.

INDEC-28 "Effects of Inhomogeneous Electron Density in a Cylindrical Plasma Column Surrounded by a Helix", R. Kalagher, Submitted to IEEE Transactions on Microwave Theory and Techniques, March 1966.

INDEC-29 "Syringe for Injecting Sodium Potassium Alloy", Samuel Greenhalgh, The Review of Scientific Instruments, Vol. 38, No. 1, pp. 121-122, January 1967.

INDEC-30 "Characteristics of Plasma Probes in a MHD Working Fluid", A. Whitman, H. Yeh, presented at International Symposium on Magnetohydrodynamic Electrical Power Generation, Salzburg, Austria, July 4-8, 1966.

INDEC-31 "Convergence of Successive Approximations to the Scalar Electrical Conductivity of Some Weakly Ionized Real Gases", S. Schweitzer, M. Mitchner, published in the A.I.A.A. Journal, Volume 5, No. 2, pp. 351-353, 1967.

INDEC-32 "The Determination of Thermal Diffusivities of Thermal Energy Storage Materials, Part 1, Solids Up To Melting Point", Han Chang, Manfred Altman, Ram Sharma. Accepted for publication in the A.S.M.E. Journal.

INDEC-33 "Electrochemical Principles of Corrosion", Leonard Nanis, presented at the National Association of Corrosion Engineers Symposium, September, 1966, Philadelphia, Penna.

INDEC-34 "Tolerance Specification by Multiple Alignment Statistics", L. Nanis, presented at Session 14 "Effective Utilization of Grid-Based Interconnection Systems", proceedings of the 1966 Western Electronic Show and Convention, Los Angeles, California, August, I.E.E.E.

INDEC-35 "On the Tensor Electrical Conductivity of Atmospheric Cesium-Seeded Argon", S. Schweitzer, accepted by the A.I.A.A. Journal for publication in May, 1967.

INDEC-36 "The Reaction of Molten Metal Droplets with a Rarefield Atmosphere", by M. Altman, D. Ross. Accepted for publication in the A.I.A.A. Journal.

INDEC-37 "Electron Transfer Processes Through Tantalum-Tantalum Oxide Diodes", S. Pollack. Journal of Applied Physics, November, 1966.

INDEC-38 "A Method for Determination of the Permeation Rate of Hydrogen Through Metal Membranes", J. McBreen, W. Beck, L. Nanis, Journal of Electrochemical Society, 113, No. 11, pp. 1218-1222 (November 1966).

INDEC-39 "Tensor Electrical Conductivity of a Partially Ionized Gas in a Magnetic Field", S. Schweitzer and M. Mitchner. To be published in the Physics of Fluids.

INDEC-40 "New Method of Producing Electric Power by Means of a Thermionic Converter". Patent applicatior. by M. Altman.

INDEC-41 "A Metal-Oxide Thin Film Photovoltaic Energy Converter". Patent application by M. Altman and S. R. Pollack.

INDEC-42 "Current & Potential Distribution in Cylindrical Geometries: Engineering Applications", L. Nanis, submitted to Journal Electrochemical Society, to be presented at Current Distribution Symposium, Dallas, May 1967 Meeting, Electrochemical Society.

INDEC-43 "Overpotential-Time Variation for Galvanostatic Charging with Potential Dependent Capacitance", L. Nanis, P. Javet, submitted to Journal Electrochemical Society, to be presented at Current Distribution Symposium, Dallas, May 1967 Meeting, Electrochemical Society.

INDEC-44 "Galvanostatic Charging with Potential Dependent Double Layer Capacitance", L. Nanis, P. Javet, to be submitted to Electrochimica Acta.

INDEC-45 "Decay of Overpotential from the Tafel Region with Potential Dependent Double Layer Capacitance", L. Nanis, P. Javet, to be submitted to Journal of Electrochemical Society.

INDEC-46 "Status of Magnetohydrodynamic Power Generation for Terrestrial Applications", H. Yeh, presented at the A.I.A.A. Third Annual Meeting in Boston, Massachusetts, Nov. 29 - Dec. 2, 1966.

INDEC-47 "First Order Effects of Production on the Continuum Theory of Spherical Electrostatic Probes", Ira M. Cohen and S. Schweitzer, February, 1967.

INDEC-48 "The Electric Automobile - A Discussion of Strategy, Tactics, and Leadership", M. Altman, presented at the National Electric Automobile Symposium, San Jose, California, Feb. 24, 25, 1967.

INDEC-49 "The Electric Automobile - Its Future", M. Altman, presented at the IEEE International Convention, New York, March 20 - 23, 1967.

MATERIALS ENGINEERING

APPENDIX

A-1

3 Thermal Diffusivity of Liquids 6

Senior Investigators: 6 Dr. Manfred Altman, Dr. Ram Sharma
Ph.D. Student: K. Sreenivasan 4

The theory and the experimental details of the method have been described in previous reports. Fundamentally, the difference between the temperature at the surface and at the center of a cylindrical container is measured for a constant rate of surface temperature rise. The liquid, whose thermal diffusivity is to be measured, is contained in an annular groove concentric with the surface. Note that it is not necessary to measure the temperature of the liquid. The width of the groove is so small as to maintain "creeping thermal motion" in the liquid. This minimizes free convection effects to a negligible value.

The thermal diffusivity of the container material is essential for calculating liquid thermal diffusivity. This report presents the experimental results for the thermal diffusivity of the container material. The experimental technique is similar to the one described above with this difference--the cylindrical container is replaced by a solid cylindrical specimen. The material of the specimen is boron nitride. The surface temperature and the difference between the surface temperature and the temperature at the center are monitored in separate recorders. The thermal diffusivity of the specimen is calculated using the recorder data. The experimental results are presented in Fig. 1.

A new 2 3/8" Dia. Pt. -40% Rh wire-wound-furnace has been designed and built. This was used for the liquid diffusivity measurements. The results are presented in the next section.

Experimental Results

It was decided to calibrate liquid-diffusivity cell by testing a liquid whose thermal diffusivity has been measured by other investigators. Sodium Nitrate (melting point 306.8^{o}C) was chosen as the liquid. Sodium Nitrate was tested in the 0.0625 inch annular gap container. The results are shown in Fig. 2. As seen in this figure, the results of this investigation compare very favourably with the results of Bloom et al (Ref. 1).

Lithium Fluoride liquid was tested in two containers whose gap widths were different, in order to detect the influence of free convection. It may be recalled that the influence of free convection is proportional to the cube of the gap width. The results obtained with both the containers are shown in Fig. 3. No discernible difference exists in these results. It is reasonable to conclude that free convection effects are negligibly small.

Ref. 1. H. Bloom, A. Doroszkowski, and S. B. Tricklebank
Australian J. Chem., 18, 1171-6, 1965.

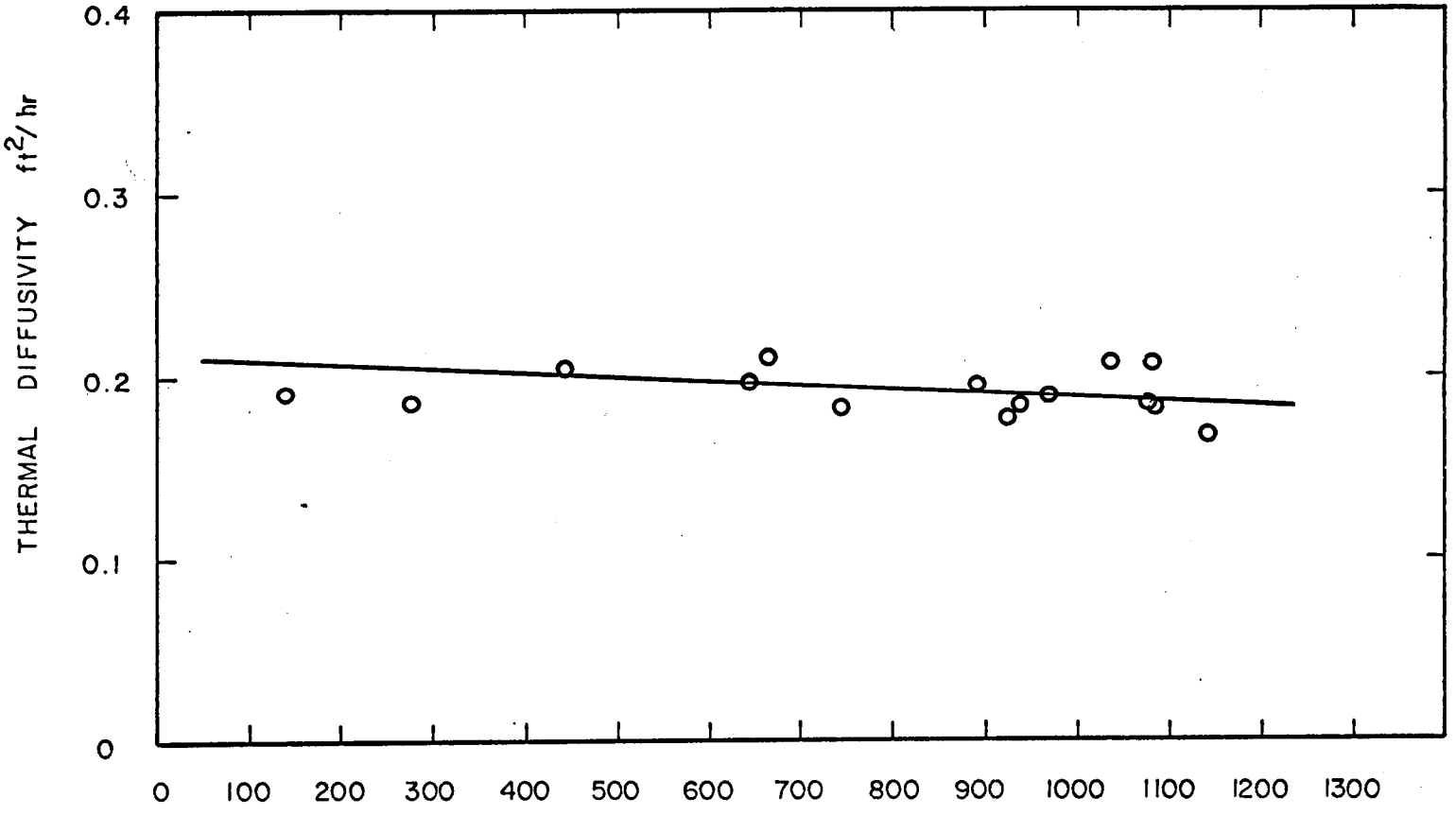

THERMAL DIFFUSIVITY OF BORON NITRIDE

FIG. 1

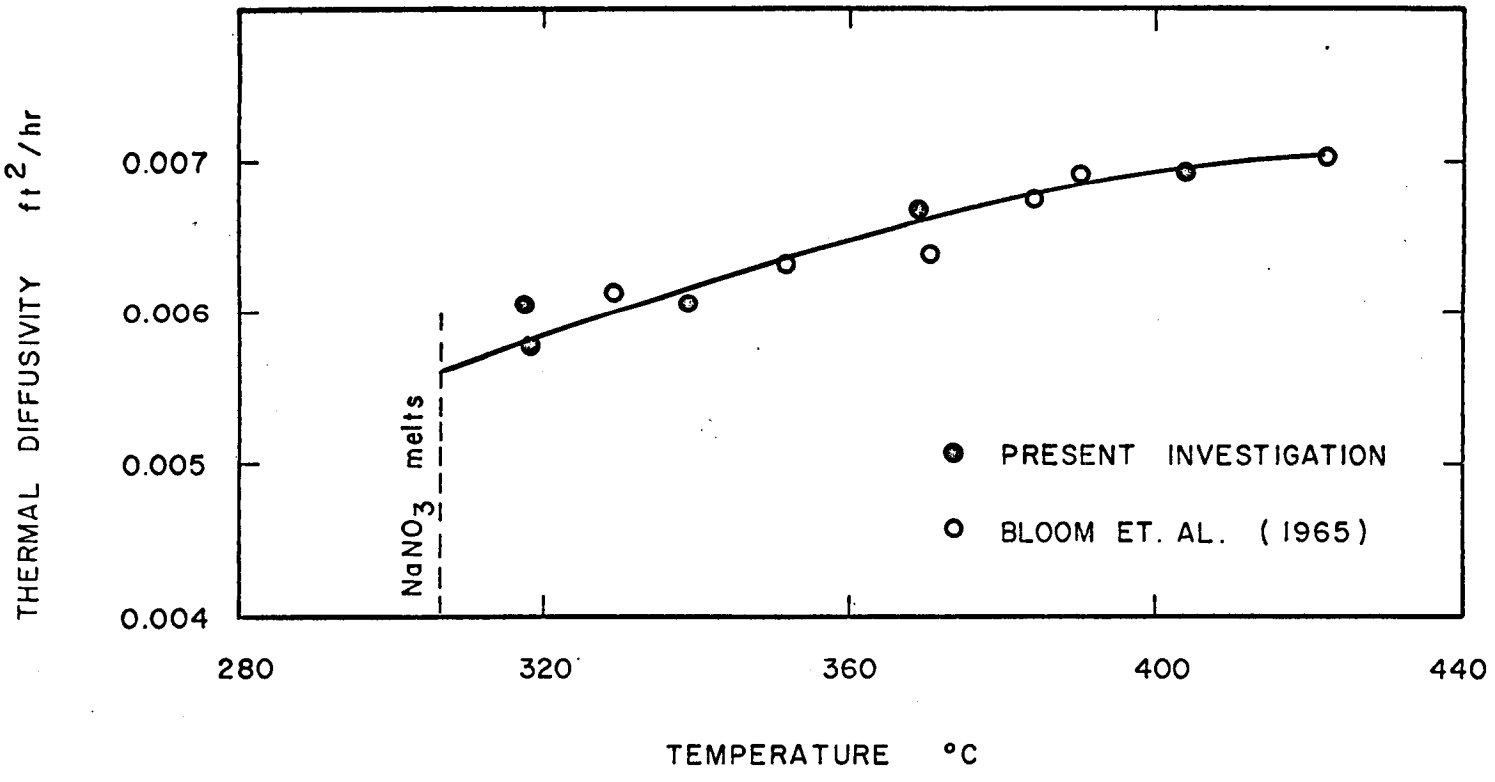

THERMAL DIFFUSIVITY OF SODIUM NITRATE

FIG. 2

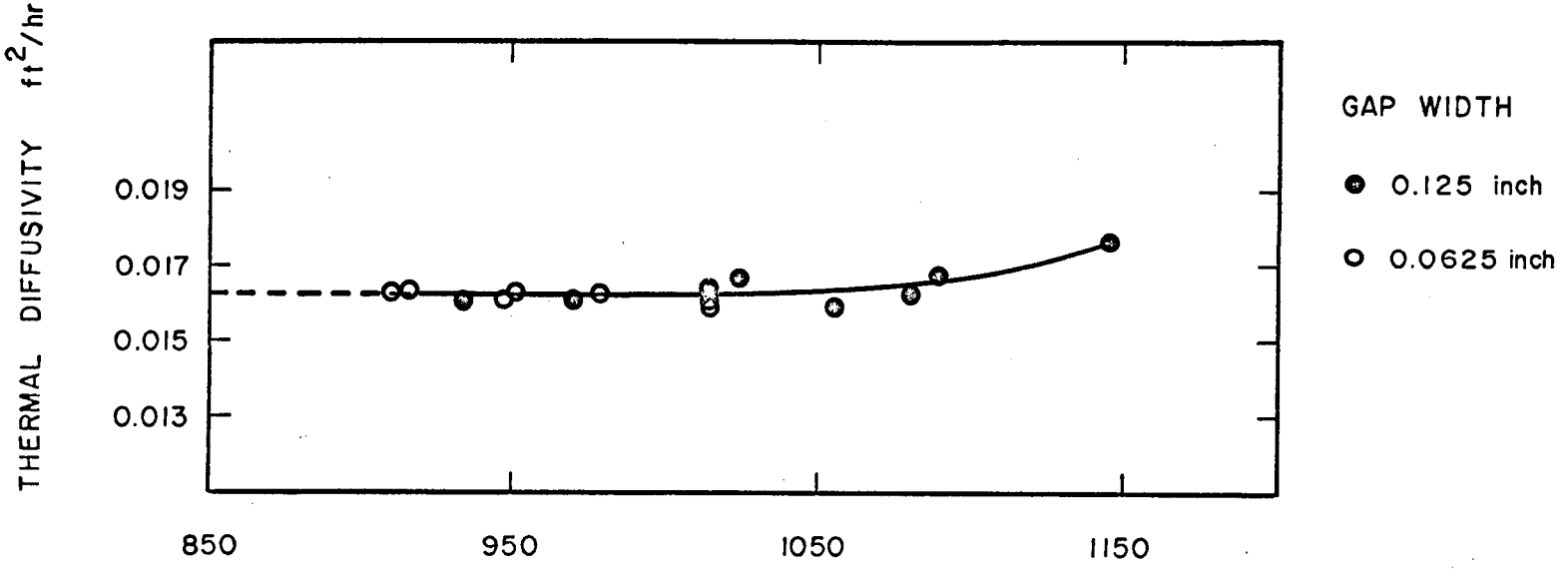

THERMAL DIFFUSIVITY OF LITHIUM FLUORIDE

FIG. 3

TABLE I

Thermal Diffusivity of CaF_2, BaF_2, and Their Mixtures

2×10^3 (cm^2/sec)

Temp (^oC)	CaF_2	BaF_2	33.3% CaF_2 +66.7% BaF_2	66.7% CaF_2+ 33.3% BaF_2
100	12.9	13.5	13.25	13.0
200	9.9	10.57	10.3	10.1
300	8.75	9.5	9.26	9.06
400	7.85	9.0	8.75	8.44
500	7.24	8.85	8.55	7.97
600	6.75	8.82	8.45	7.59
800	6.25	8.78	8.36	7.25
1000	6.13	8.78	8.36	7.22

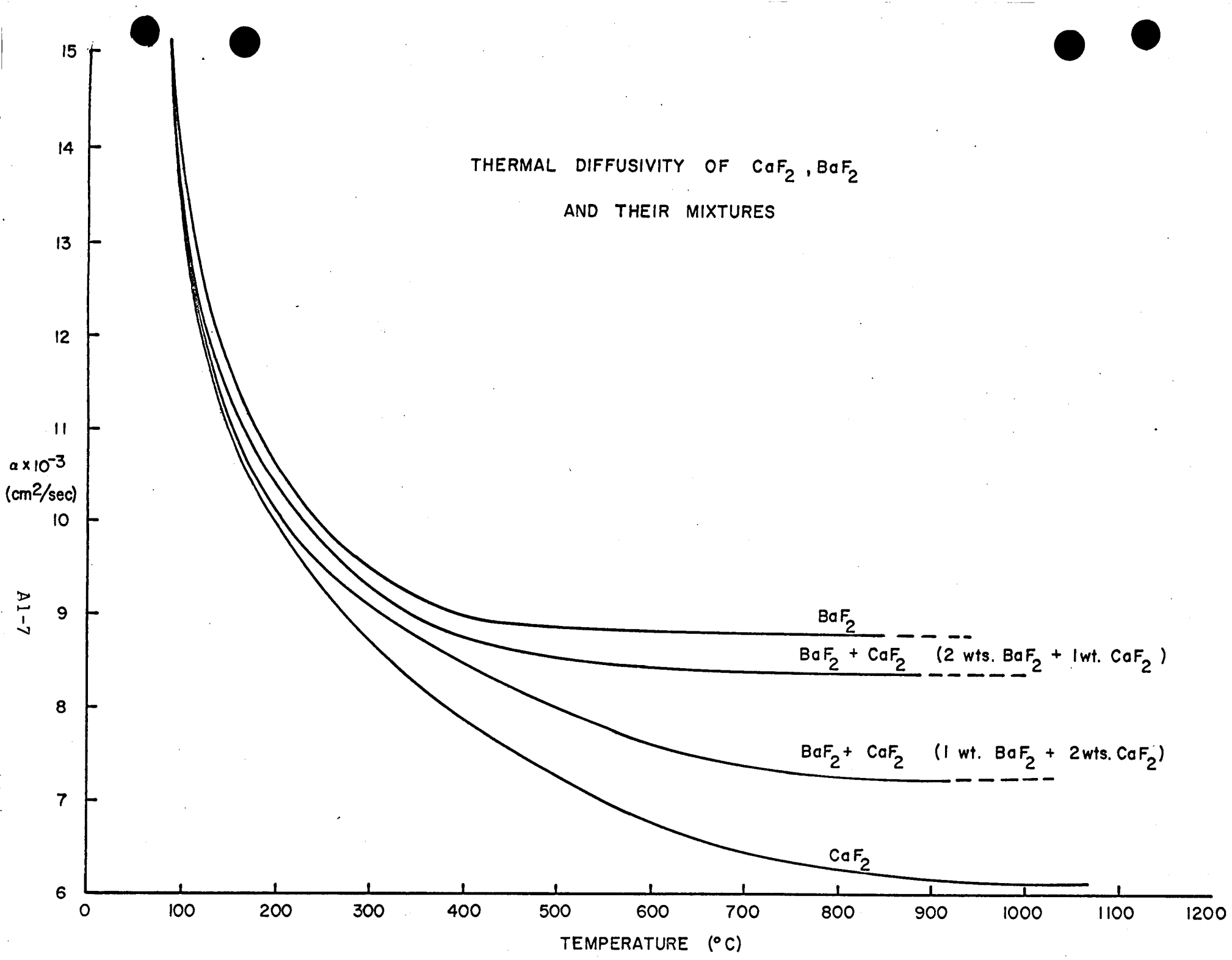
THERMAL DIFFUSIVITY OF CaF_2, BaF_2
AND THEIR MIXTURES
$\alpha \times 10^{-3}$
(cm^2/sec)
15
14
13
12
11
10
9
8
7
6
0
100
200
300
400
500
600
700
800
900
1000
1100
1200
TEMPERATURE (°C)
BaF_2
$BaF_2 + CaF_2$ (2 wts. BaF_2 + 1wt. CaF_2)
$BaF_2 + CaF_2$ (1 wt. BaF_2 + 2wts. CaF_2)
CaF_2

3 Experimental Determination of the Thermoelectric Properties of Graphite Alloys 6

Senior Investigator: 6 Dr. S. R. Pollack

Graduate Student: J. J. Curry 4

During the past quarter, the apparatus for the measurement of the thermoelectric power, electrical conductivity, Hall coefficient and magnetoresistivity has been completed. The apparatus has been checked and calibrated thoroughly. Measurements of the thermoelectric power of silver as a function of temperature have been made. The reproducibility and agreement with published experimental results are excellent.

Since the instrumentation has been completed and the graphite compounds have not been available in large enough quantities to permit measurements of the thermoelectric properties, work has begun on the study of some semiconductor compounds. These compounds belong to a class of compounds $Cu\text{-}2_2\text{-}3\text{-}6_4$ where the numbers designate the period of the components on the periodic chart. This class of compounds has been developed by Professor E. Parthé of the Metallurgical Engineering faculty, and Professor Parthé has agreed to collaborate with us on this project. The structure of the compounds is tetrahedral and of the zincblende type.

Several samples were prepared from commercially pure elements and tested. Of these, one compound, $CuCd_2In\,Te_4$, seemed extremely promising. The compound has a lattice parameter of 6.34Å with a c/a ratio of 2. The thermoelectric power was very high ($+340\mu v/^{\circ}K$ @$300^{\circ}K$). The electrical conductivity was 10^{-2} to 10^{-4} $(ohm\text{-}cm)^{-1}$ depending on heat treatment.

Six other samples were prepared using both commercially pure

and hi-purity elements. We were unable to duplicate the crystal structure of the previous compound. However, one sample of hi-purity materials was composed of $CuCd_2InTe_4$ plus a small quantity of some other phase. Measurements on this sample indicated that the thermoelectric power was reduced to $+85\mu v/^{o}K@300^{o}K$ and had an electrical conductivity of 2.38 $(ohm-cm)^{-1}$.

It is believed that the high thermoelectric power is due to an impurity effect. If one assumes that $N_A \leq N_D$, where N_A and N_D are respectively the concentration of acceptors and donors, in the sample made with commercial purity, then the Fermi level should be close to the center of the forbidden gap but below it. This should result in a large thermoelectric power and a moderate p-type conductivity as observed. However, when the compound is made from hi-purity elements, the donor concentration is reduced. This brings the Fermi level closer to the acceptor level. Although this brings about an increase in the p-type conductivity, it reduces the thermoelectric power due to the lowering of the Fermi level.

Current programs entail the determination of the impurities and the measurement of the absorption band gap by optical techniques. Studies will be made on compounds of various dopant concentrations and the effects of heat treatment on the thermoelectric properties. New methods will be developed for compound preparation in order to enhance the reproducibility and make the preparation more efficient.

3 Tunnel Emission Cold Cathodes 6

Senior Investigator: Dr. S. R. Pollack

Graduate Student: S. Basavaiah

Vacuum System:

Varian vacuum chamber and the accessories were delivered during the first week of November. The vacuum system was assembled by the middle of November and appropriate performance checks were made. The system performance is as follows:

Roughing time from atmosphere to 2×10^{-4} Torr. is 20 minutes as compared to an hour for the previous Elion System. Total time to achieve 5×10^{-8} Torr. is approximately 2 hours compared to 2 days for the previous system. Ultimate vacuum achieved is 5×10^{-9} Torr.

Necessary fixtures for thin film evaporation were incorporated.

Sample Preparation:

Tungsten - Tungsten Oxide - Gold tunnel junctions are fabricated as follows:

99.999 pure zone refined tungsten is evaporated by "Electron Beam Evaporation" onto a 3"x1" glass (7059 Corning) substrate at a pressure of 5×10^{-6} Torr. This is not the best that can be done. It merely represents the convenient pressure for preliminary experiments. The pressure at the start of the evaporation is 5×10^{-8} Torr. The evaporation rate is approximately $20 A^{\circ}$/minute. This is estimated by dividing the thickness by the total time of evaporation. Due to the delay in the delivery of crystals, the quartz crystal microbalance could not be used at this stage.

The tungsten film is oxidized by plasma oxidation at an oxygen pressure of 55 microns. The discharge voltage is 600 volts with a distance

of approximately 1 1/2" between the cathode and anode. The sample is kept in the negative glow of the discharge for 15 minutes.

Gold films are evaporated onto the oxidized tungsten film at right angles to it.

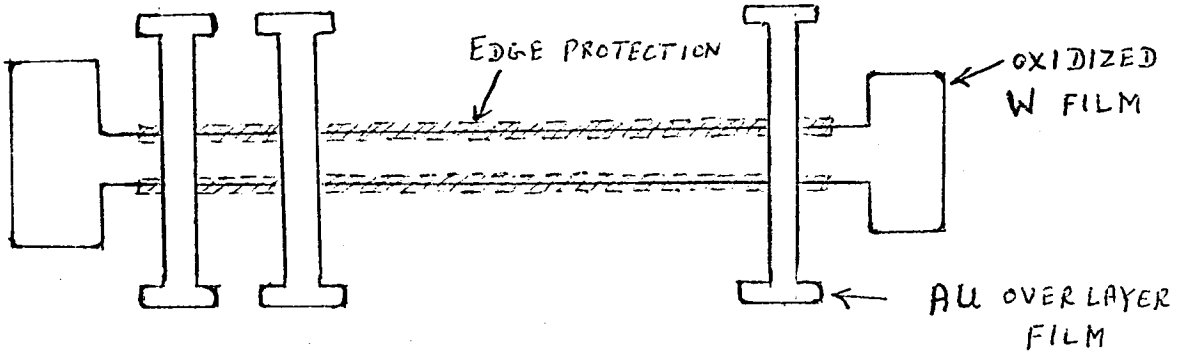

Fig. 1

MEASUREMENTS AND DATA:

Current-voltage (V-I). Characteristics of the samples are being taken. This being the first set of samples, no firm conclusions can be drawn at this stage, but a rough idea of the behaviour can be obtained.

Figure 2 is a typical V-I characteristic.

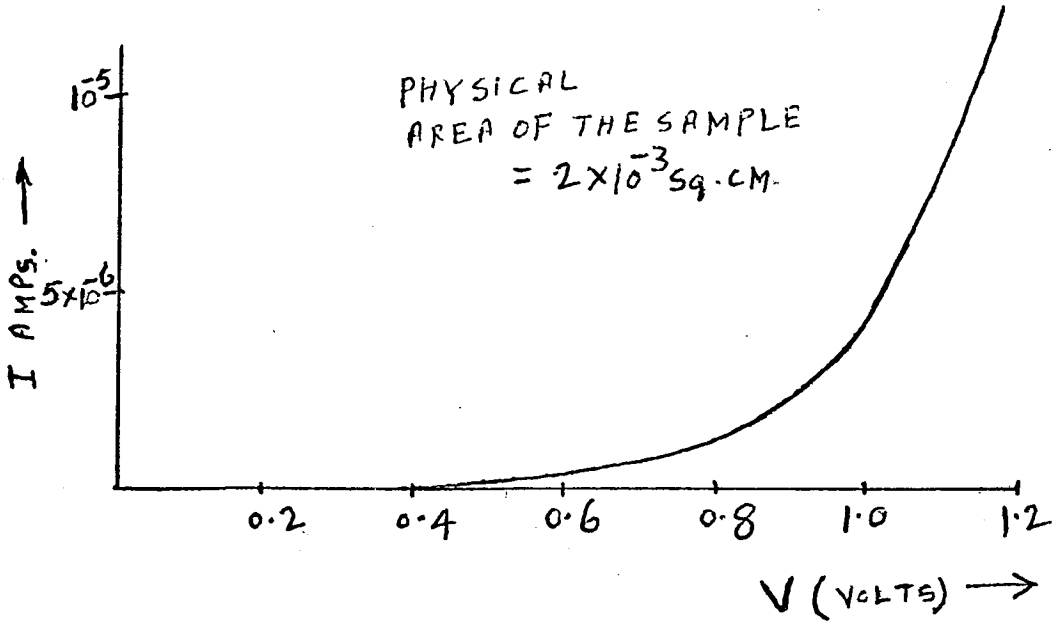

Fig. 2

The capacitance of the sample was measured by a bridge and assuming a dielectric constant of 41.7 for tungsten oxide, the thickness of the oxide is estimated to be 95A°.

Further Plans:

Dr. Pollack had discussions with Dr. A. Goodman of R.C.A. Laboratory in Princeton concerning the possibility of collaboration in the internal photo emission measurements on the samples. Dr. Goodman was anxious to collaborate and his department head, Dr. Paul Rappaport, was also enthusiastic. This collaboration is being further studied.

Further investigations are under way. These include:

1) Mask design to eliminate edge effects.
2) Mask design to include samples for internal photo emission measurements.
3) Detailed I-V-T measurements from 77°K to 200°C (if possible).
4) Attempts to identify the mechanism of electron transfer.
5) Determination of barrier heights with different over layer metal films.

3 Studies of Thermal Transpiration for the Development of a "Thermal Pump" 6

6 Dr. M. Altman Mr. E. Hopfinger 8

The phenomena of thermal transpiration was described in the previous report, and flow rates through an infinitely thin membrane, calculated from kinetic theory, have been presented. It was also mentioned that in an experimental setup, the flow will be governed by diffusion rather than effusion, and therefore, much lower flow rates than the ones shown in the graph of the previous report are to be expected.

The experimental setup has now reached a stage where preliminary data could be taken. In this apparatus the membrane is sealed in by a silicone rubber gasket, which limits the temperature to <250°C. Helium was used for these preliminary runs and the membrane (porcelain) specifications were: 38.5 cm^2 effective area, 0.55 cm thick, 0.3×10^{-6} cm average pore diameter, 58% porosity. In one run, the surface temperatures of the membrane were 225°C at the hot side, and 31°C at the cold side.

At various mean pressures $\bar{p} = 1/2\ (p_H + p_C)$, the maximum pressure difference $\Delta p = p_H - p_C$ (after about 5 min.), and the flow rates were recorded, keeping the temperature difference $\Delta T = T_H - T_C = 194°C$ constant to within $\pm$ 2%, except at $\bar{p}$ <3 cm Hg where the cold side temperature increased to 41°C at $\bar{p}$ = 1.04 cm Hg. The pressure difference was displayed on a differential mercury manometer and the flow rates on a mercury column displacement flow meter, which needed <1 mm Hg pressure drop when lubricated with sulfuric acid.

The results are presented in Figs. 1 to 3. Fig. 1 shows the flow rates of Helium in gr./min. x cm^2 membrane area. A comparison with the flow rates through an infinitely thin membrane has not much meaning,

especially at this stage, but if the ratio of the flow rates at $\Delta T=194^{o}C$ and atmospheric pressures is taken, a factor of 10^{5} is obtained, assuming a ratio of cm^{2} membrane area to be cm^{2} pore area of 6/1.

In Fig. 2 the ratio of grams gas circulated to grams in system (which is directly proportional to the gas concentrations in the membrane) is plotted versus $\bar{p}$. This curve has a maximum at $dav./\lambda \cong .2$, which probably indicates that this is the ratio for optimum flow rates.

Figure 3 shows the pressure ratio to temperature ratio versus mean pore diameter to mean free path ratio. This should approach 1 at $dav/\lambda << 1$ and .781 at $dav/\lambda >> 1$.

In another run the flow rates and maximum pressure differences were recorded at various temperature differences, and constant mean pressure. Fig. 4 shows Δp max. and the flow rates versus ΔT at atmospheric pressure. The cold side temperature was kept constant at $T_C = T_C = 33^{o}C \pm 3\%$.

At present the apparatus is modified to permit isothermal flow rate measurements which are essential for the theoretical interpretation of the data.

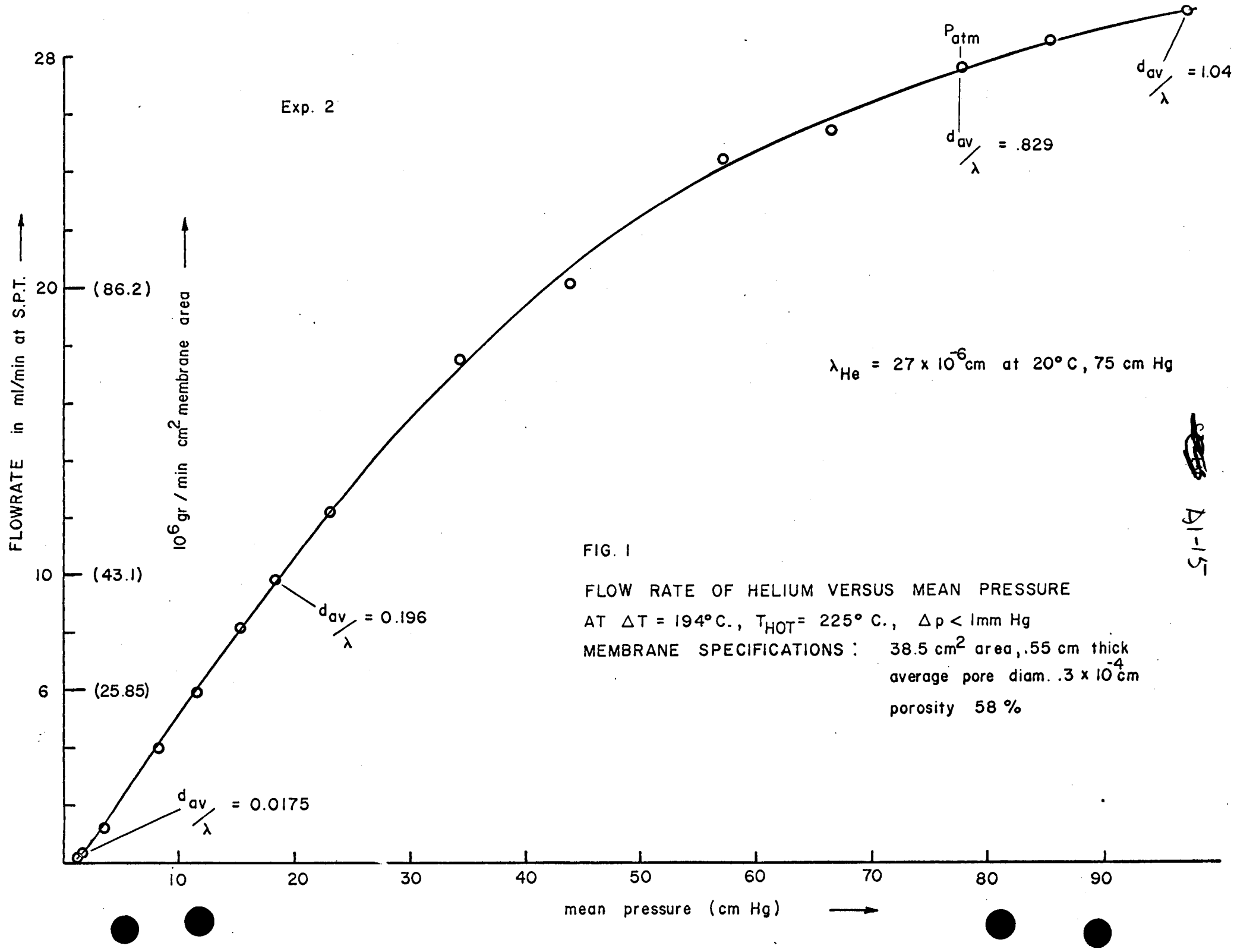

FIG. 1

FLOW RATE OF HELIUM VERSUS MEAN PRESSURE
AT ΔT = 194° C., T_{HOT} = 225° C., Δp < 1mm Hg
MEMBRANE SPECIFICATIONS : 38.5 cm^2 area, .55 cm thick
average pore diam. .3 x 10^{-4} cm
porosity 58 %

A1-15

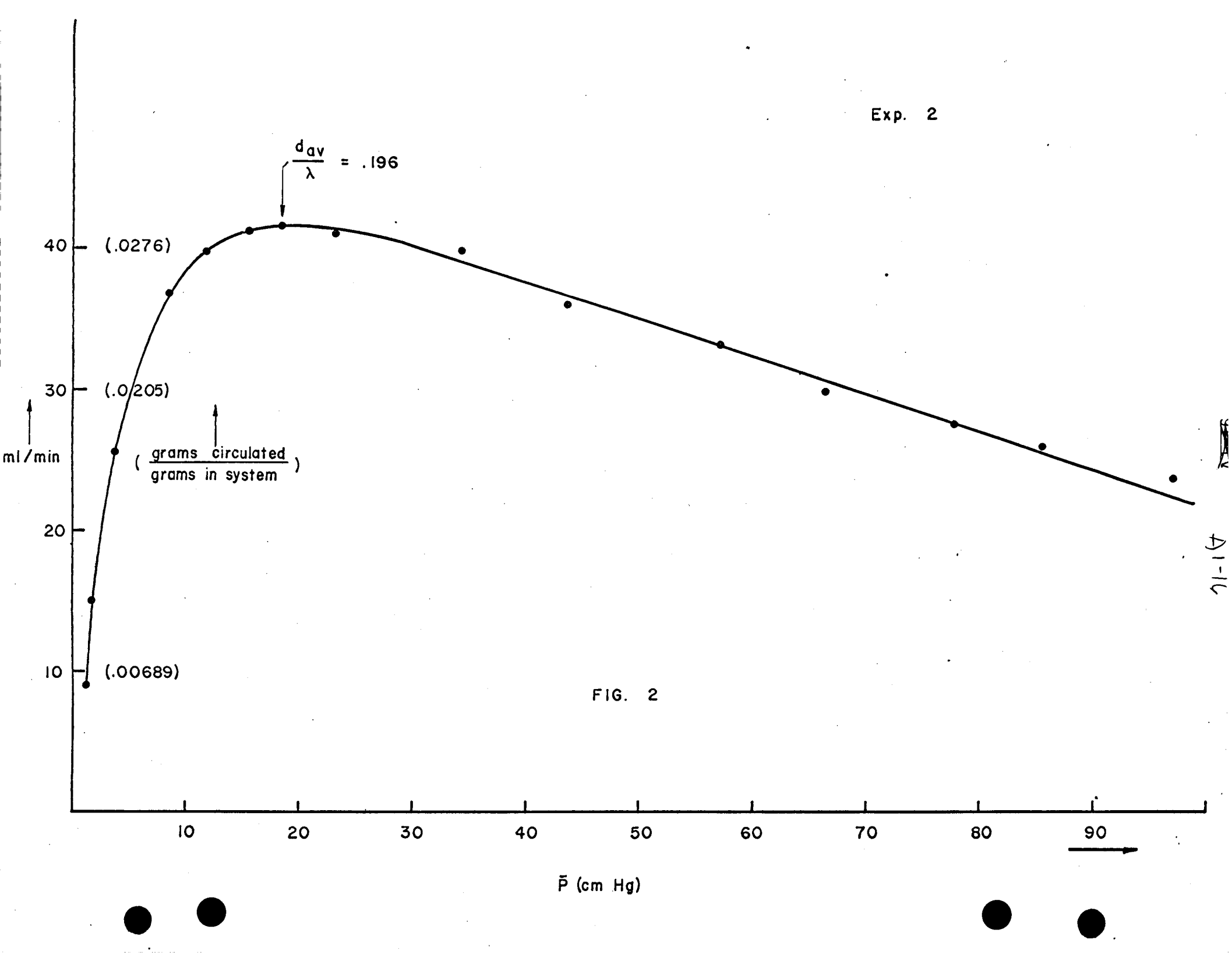
Exp. 2
$\frac{d_{av}}{\lambda}$ = .196
40
(.0276)
30
(.0205)
20
10
(.00689)
ml/min
(grams circulated / grams in system)
10
20
30
40
50
60
70
80
90
$\bar{P}$ (cm Hg)

FIG. 2

A1-1C

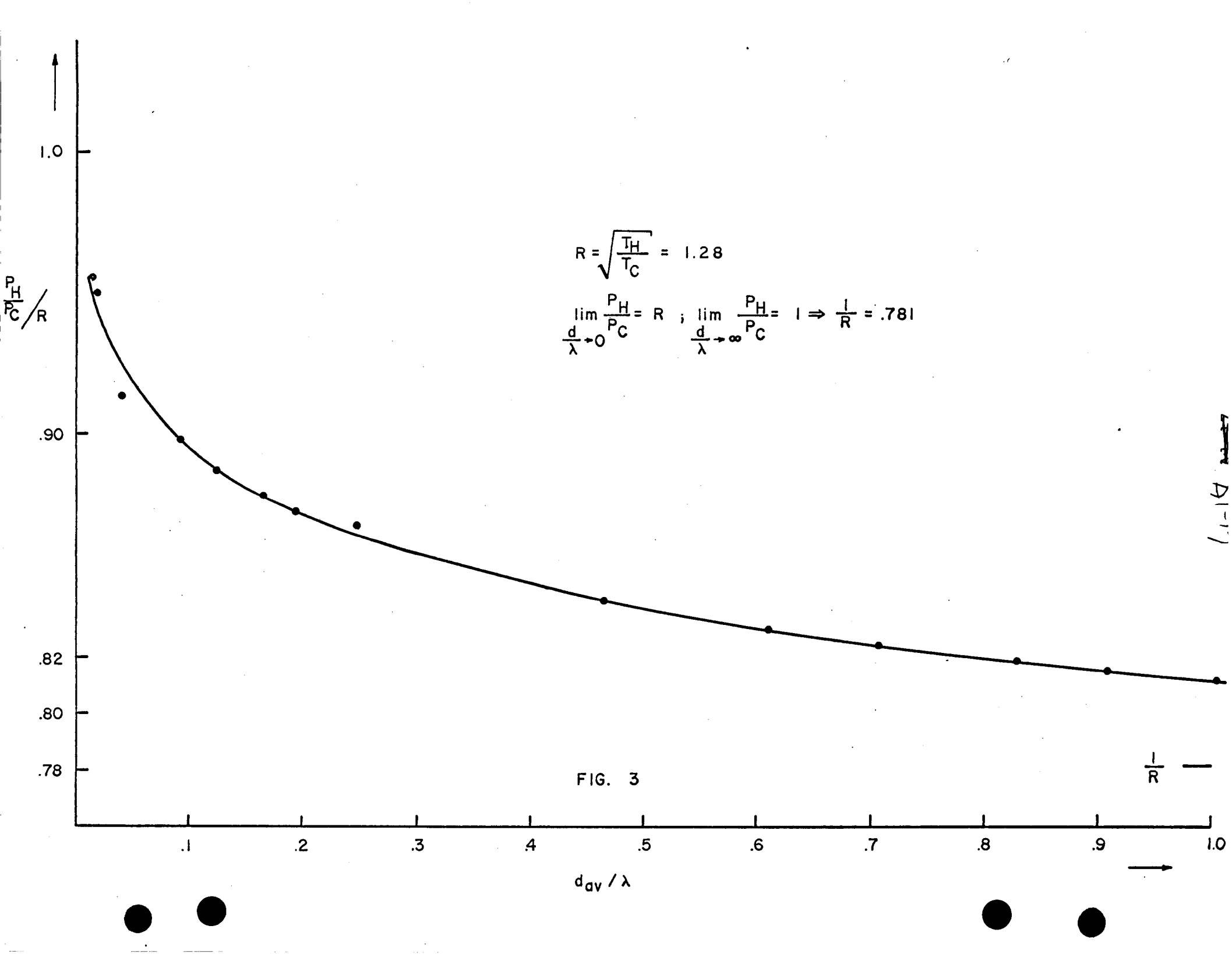
1.0
.90
.82
.80
.78
$\frac{P_H}{P_C}/R$
$R = \sqrt{\frac{T_H}{T_C}} = 1.28$
$\lim_{\frac{d}{\lambda}\to 0} \frac{P_H}{P_C} = R$; $\lim_{\frac{d}{\lambda}\to \infty} \frac{P_H}{P_C} = 1 \Rightarrow \frac{1}{R} = .781$
$\frac{1}{R}$
.1
.2
.3
.4
.5
.6
.7
.8
.9
1.0
d_{av}/λ

FIG. 3

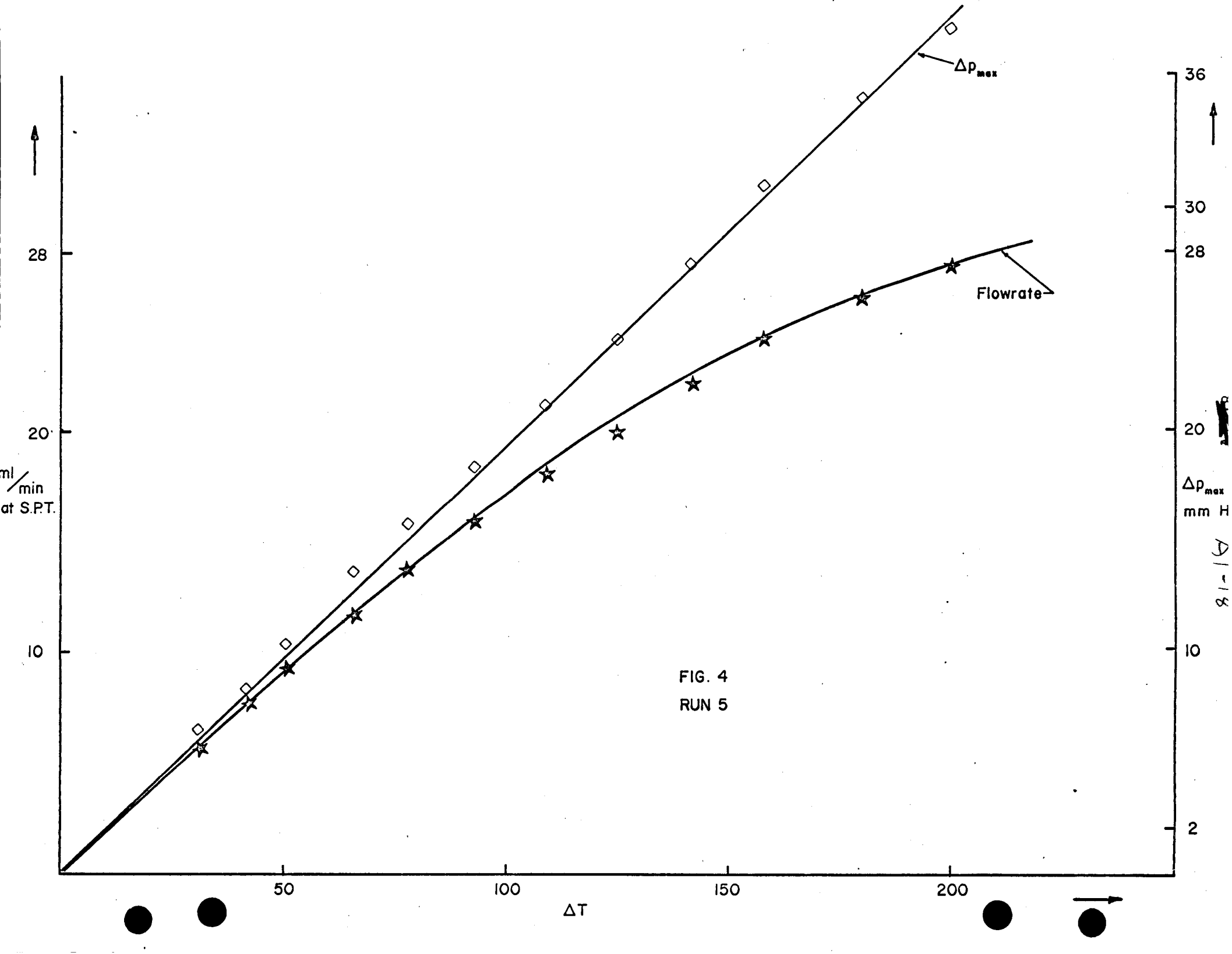
Δp_{max}
Flowrate
36
30
28
20
10
2
28
20
10
ml/min at S.P.T.
Δp_{max} mm H
50
100
150
200
ΔT

FIG. 4
RUN 5

PLASMA ENGINEERING

APPENDIX

A-2

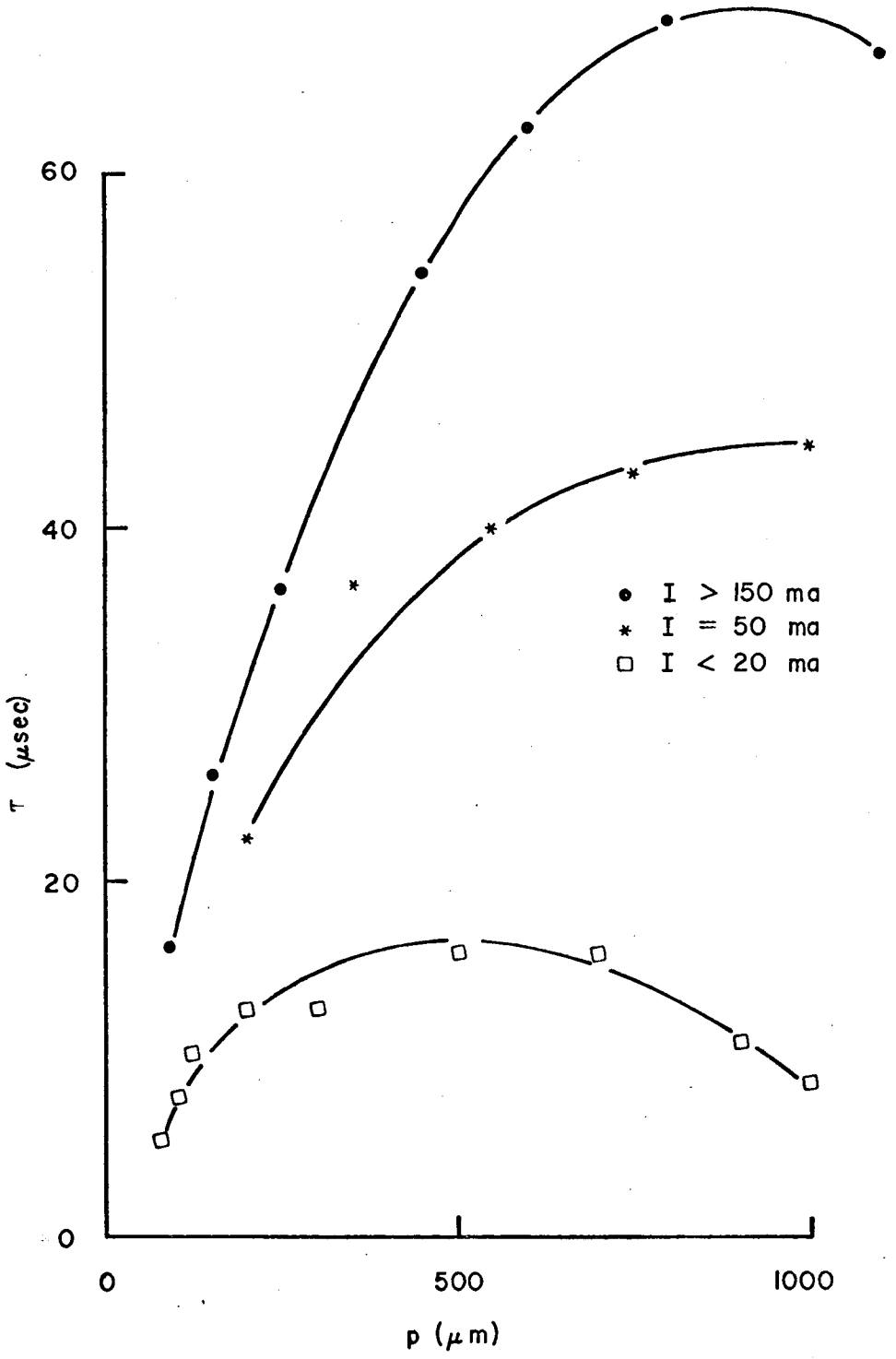

f = 8.20 GHz , PRF = 200 Hz

DECAY CONSTANT IN AFTERGLOW ARGON PLASMA

Fig. 1

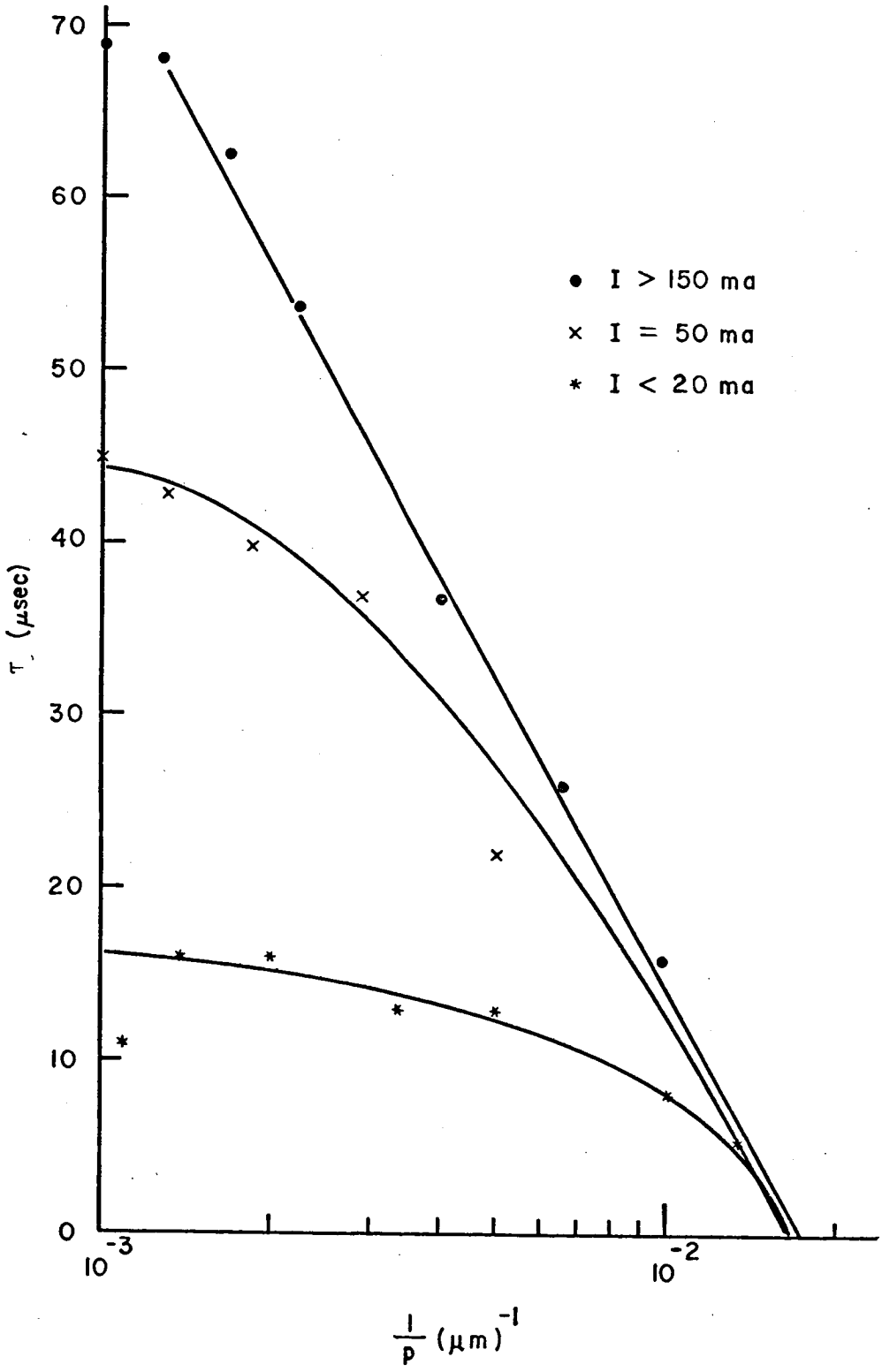

DECAY CONSTANT IN AFTERGLOW ARGON PLASMA

Fig. 2

Flow of a Conducting Liquid in an Annular Gap: A Restricted Nonexistence Proof

by

S. Schweitzer* and I. M. Cohen*
University of Pennsylvania
Philadelphia, Pennsylvania

We consider the problem of a liquid conductor (such as Mercury) confined between two concentric cylindrical electrodes. The liquid metal is electromagnetically accelerated by the Lorentz force in the circumferential direction created when a current is passed between the two electrodes (held at different potentials) and an axial magnetic field is applied. The governing equations are the coupled momentum and Maxwell equations together with Ohm's law in the special case of steady state, inviscid flow with constant properties. Axial symmetry is also assumed. Gravity body forces have been neglected. The equations in vector form are then:

$$\nabla \cdot \underline{V} = 0 \qquad \text{(conservation of mass)} \qquad (1)$$

$$\nabla \cdot \underline{B} = 0 \qquad \text{(conservation of magnetic flux)} \qquad (2)$$

$$\nabla \times \underline{B} = \mu \underline{J} \qquad \text{(Ampere's law)} \qquad (3)$$

$$\nabla \times \underline{E} = 0 \qquad \text{(Faraday's law)} \qquad (4)$$

$$\underline{J} = \sigma (\underline{E} + \underline{V} \times \underline{B}) \qquad \text{(Ohm's law)} \qquad (5)$$

$$\nabla \tfrac{1}{2} V^2 - \underline{V} \times (\nabla \times \underline{V}) = -\nabla p/\rho + (1/\rho)(\underline{J} \times \underline{B}) \qquad \text{(conservation of momentum)} \qquad (6)$$

Combining Eqs. (3) and (6) gives the "momentum eq.", and (3), (4), (5) gives the "magnetic eq.". Thus, we have:

$$\nabla \cdot \underline{V} = 0 \qquad (7)$$

---

*Assistant Professor. Member AIAA.

This work has been supported by the Institute for Direct Energy Conversion and the Towne School of Civil and Mechanical Engineering at the University of Pennsylvania.

$$\nabla \cdot \underline{B} = 0 \tag{8}$$

$$\nabla \times (\underline{B} \times \underline{V}) + (1/\mu\sigma)\ \nabla \times (\nabla \times \underline{B}) = 0 \quad \text{(magnetic equation)} \tag{9}$$

$$\nabla\ \tfrac{1}{2}\ V^2 - \underline{V} \times (\nabla \times \underline{V}) = -\nabla p/\rho + (1/\rho\,\mu)(\nabla \times \underline{B}) \times \underline{B}$$

$$\text{(momentum equation)} \tag{10}$$

with the boundary conditions:

(1) $\phi_o = -\int_{r_1}^{r_2} \left[(1/\mu\sigma) \cdot (\partial B_\theta/\partial z) + v_\theta B_z\right] dr$ for all z

(2) $B_\theta = 0$ at $z = L$, $B_\theta = \mu I/2\pi r$ at $z = -L$, $I \neq 0$.

(3) $E_z = 0$ at $r = r_1, r_2 \Rightarrow v_\theta B_r = (1/\mu\sigma r)\ \partial/\partial r\ (r B_\theta)$ at $r = r_1, r_2$

(4) $E_\theta = 0$ at $r = r_1, r_2 \Rightarrow \partial B_r/\partial z - \partial B_z/\partial r = 0$ at $r = r_1, r_2$

where $\underline{B}$ is the magnetic induction, $\underline{v}$ is the velocity of the fluid, μ is the magnetic permeability, σ is the electrical conductivity, p is the pressure, ϕ_o is the potential difference between the two electrodes. We have also assumed that there is no secondary flow.

The boundary conditions are consequences of the following physical considerations. Boundary condition (1) is a statement that the difference in potential between the inner and outer electrodes is ϕ_o, which is a line integral of $\underline{E}$ from one electrode to the other and independent of the path by virtue of Eq. (4). We have chosen a radial path for the line integral and $\underline{E}$ has been replaced by its value through Ohm's law and $\underline{J}$ has been replaced by curl $\underline{B}$ through Ampere's law. Boundary condition (2) is found from the integral form of Ampere's law and states that all of the current comes in from the bottom and none leaves through the top. (See the Figure.) This is consistent with insulated end plates, $J_z = 0$ at $z = \pm L$. Assuming that the electrodes are perfect conductors, $\underline{E}$ must be radial at the electrode surfaces. Then Ohm's law together with $\underline{v} = v_\theta \underline{1}_\theta$ and $\underline{J}$ replaced by curl $\underline{B}$ yields

boundary conditions (3) and (4). For arbitrary values of the physical parameters, the equations split up into autonomous subsystems, i.e., the magnetic field may be solved for independently of the flow and the coupling between the magnetic and velocity fields enters through the boundary conditions. We prove here a restricted nonexistence theorem: under the assumptions (a) $B_z = \text{const.}$, (b) $B_r = 0$, or (c) $rB_\theta = f(z)$, no solutions of the above equations and boundary conditions exist.

In scalar, component form, the equations become

$$\partial v_\theta/\partial\theta = 0, \text{ conservation of mass } (\underline{v} = \underline{1}_\theta v_\theta \text{ only because secondary flow is neglected}) \tag{11}$$

$$(1/r)\,\partial/\partial r\,(r B_r) + \partial B_z/\partial z = 0, \quad \text{conservation of magnetic flux} \tag{12}$$

$$\partial/\partial z\,(\partial B_r/\partial z - \partial B_z/\partial r) = 0, \quad r \text{ - magnetic eq.} \tag{13}$$

$$\partial/\partial r\left[r\,(\partial B_z/\partial r - \partial B_r/\partial z)\right] = 0, \; z \text{ - magnetic eq.} \tag{14}$$

$$-\partial^2 B_\theta/\partial z^2 - \partial/\partial r\left[(1/r)\,\partial/\partial r\,(r B_\theta)\right] = \mu\sigma\left[\partial/\partial z\,(v_\theta B_z) + \partial/\partial r\,(v_\theta B_r)\right] \tag{15}$$

θ - magnetic eq.

$$-v_\theta^2/r = -(1/\rho)\,\partial p/\partial r + (1/\rho\mu)\left[B_z\,(\partial B_r/\partial z - \partial B_z/\partial r) - (B_\theta/r)\,\partial/\partial r\,(r B_\theta)\right] \tag{16}$$

r - momentum eq.

$$B_z\,\partial B_\theta/\partial z + (B_r/r)\,\partial/\partial r\,(r B_\theta) = 0, \quad \theta \text{ - momentum eq.} \tag{17}$$

$$0 = (1/\rho)\,\partial p/\partial z + (1/\rho\mu)\left[B_\theta\,\partial B_\theta/\partial z + B_r\,\partial B_r/\partial z - B_r\,\partial B_z/\partial r\right], \quad z \text{ - momentum eq.} \tag{18}$$

with boundary conditions (1) - (4).

Eqs. (13) and (14) with boundary condition (4) yield

$$\partial B_z/\partial r - \partial B_r/\partial_z = 0, \quad r + z \text{ magnetic eq.} \tag{19}$$

This proves that $J_\theta = 0$ (Eq. (19) is the θ component of curl $\underline{B}$). We observe that this result is independent of the form of the momentum equation and, therefore, is valid for viscous flow as well. Thus the assumption that $J_\theta = 0$ often made[1,2,3] is here proved as a consequence of the boundary condition that $E_\theta = 0$ at the electrodes (which merely assumes that the electrodes are perfect conductors) and Eqs. (3, 4, 5).

Eq. (19) replaces Eqs. (13), (14) and B.C. (4). Note that Eqs. (19) and (12) form an autonomous subsystem for B_r and B_z, and the results may then be put into Eq. (17) for B_θ.

We shall now prove nonexistence of solutions in three cases under assumptions that are made frequently in treating the viscous problem[1,2,3].

(a) $B_z = \text{const.} = B_o$

From Eq. (19), B_r is a function of r only and Eq. (12) gives $B_r = C_1/r$, ($C_1 = \text{const.}$). Eq. (17) becomes

$$B_o \, \partial B_\theta/\partial z + (C_1/r^2) \, \partial/\partial r \, (r B_\theta) = 0$$

This has the general solution

$r B_\theta = f(z - B_o r^2/2 C_1)$, f an arbitrary function.

For no choice of f can we satisfy B.C. (2). Therefore, no solution exists where $B_z = \text{const.}$

(b) $B_r = 0$

From Eq. (17) if $B_z \neq 0$, $B_r = 0$ implies $\partial B_\theta / \partial z = 0$. But from boundary condition (2), B_θ must be a function of z. Therefore, no solution exists with $B_r = 0$.

(c) $rB_\theta = f(z)$

From Eq. (17), if $B_z \neq 0$, $rB_\theta = f(z)$ implies $\partial / \partial r (rB_\theta) = 0$ and thus $\partial B_\theta / \partial z = 0$. But from B.C. (2), B_θ must be a function of z. Therefore, no solution exists with $rB_\theta = f(z)$.

This indicates that the assumptions listed above which have been used to treat the viscous problem should be regarded with caution.

REFERENCES

1. Chang, C. C., and Lundgren, T. S., "Flow of an incompressible fluid in a hydromagnetic capacitor," Phys. Fluids 2, 627-632 (1959).

2. Gross, R. A., and Kessey, K. O., "Magnetohydrodynamic species separation in a gaseous nuclear rocket," AIAA J. 2, 295-301 (1964).

3. Kessey, K. O., "Rotating electrically conducting fluids in a long cylinder," AIAA J. 2, 864-871 (1964).

FIGURE CAPTION

Sketch of the annular gap and geometric configuration.

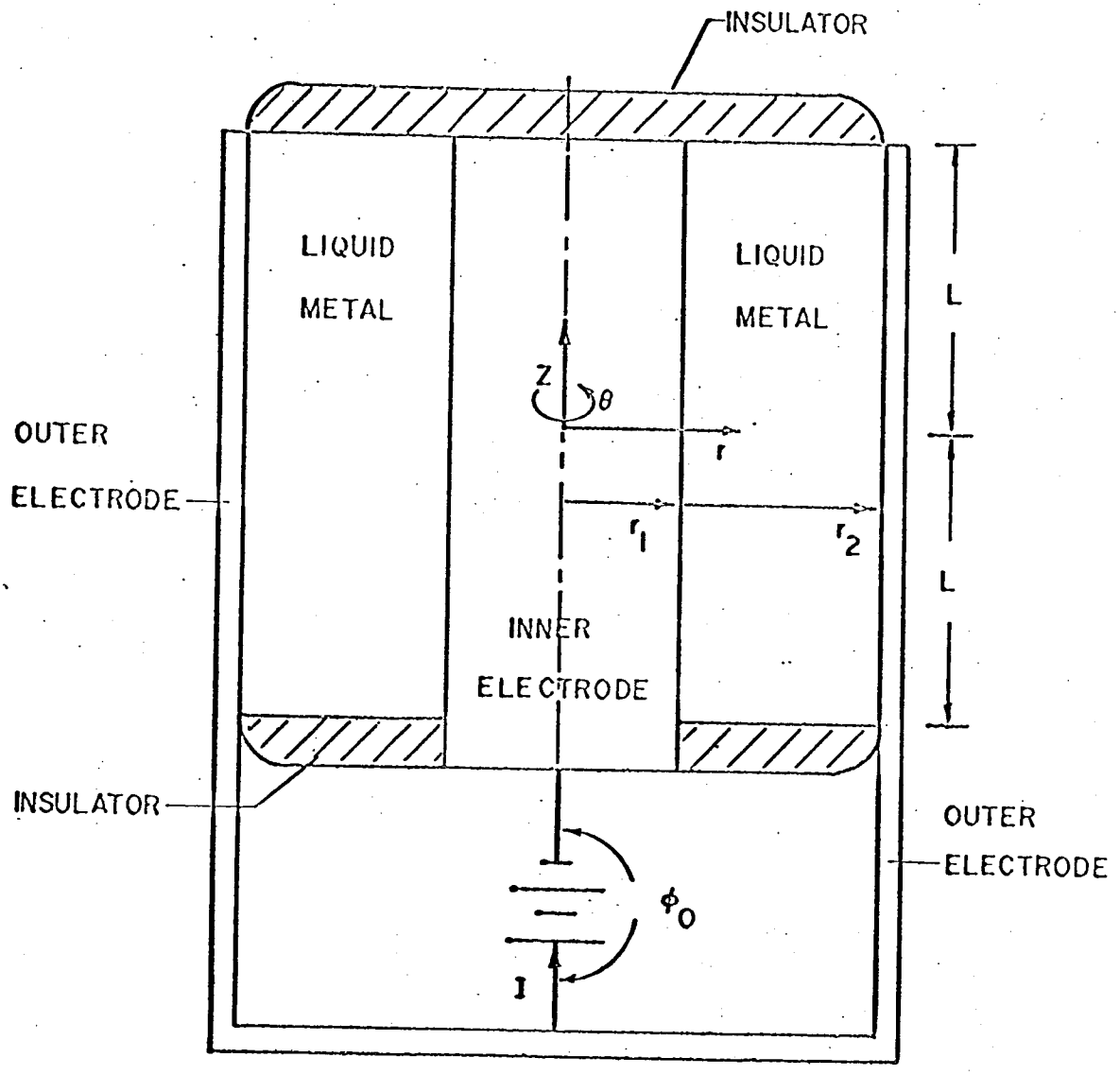
INSULATOR
LIQUID
METAL
LIQUID
METAL
OUTER
ELECTRODE
z
θ
r
r1
r2
L
L
INNER
ELECTRODE
INSULATOR
OUTER
ELECTRODE
φ0
I

3 Anistropy of Metal Work Functions 6

6 M. Kaplit 9

In order to explain the difference of at least 0.6 ev between the work function of the (110) plane of tungsten as measured by thermionic techniques ($\approx$ 5.2 ev) and field emission probe tube techniques ($\geq$ 5.8 ev), a study of the anisotropy of the electronic work function of metals for both zero electric field and extremely high electric fields (0.1 V/Å to 10 V/Å perpendicular to the surface was initiated nine months ago. The final results of this study for uniform surfaces are presented here.

Smoluchowski[1] has provided the only picture for describing the work function differences between various planes consistent with experiments: this picture is extended here to include electric spin interaction and applied electric fields. The work function is assumed to be the sum of a volume contribution and a contribution due to the surface double layer. The latter is a function of the surface plane and can be described in the following way. Every atom can be associated with a cellular polyhedron composed of all points nearer to this particular atom than to any other atom. Since the charge distribution in a surface cellular polyhedron differs from one in the bulk, a surface double layer is obtained. Two effects cause a redistribution of charge in the surface cellular polyhedrons. The spread of charge is approximately isotropic and is associated with the bulk contribution to the work function. Because of charge smoothing the surfaces of equal charge density are more nearly planar than before. The two effects have opposite influences and are comparable in magnitude, necessitating numerical computation. Applied electric fields influence primarily the degree of smoothing while electron spin interactions decrease the spreading.

The work function differences between four planes of tungsten ((110), (211), (100), (111)) were calculated for various values of the free electron density per atom F_σ - see Figure 1. For $F_\sigma \geq 0.6$, the work functions decrease in the proper experimentally verified sequence $\phi_{110} > \phi_{211} > \phi_{100} > \phi_{111}$ whereas for $F_\sigma < 0.6$ the incorrect sequence $\phi_{110} > \phi_{100} > \phi_{211} > \phi_{111}$ was obtained, indicating that Smoluchowski's linear extrapolation to $F_\sigma = 1/6$[1] was not mathematically correct. However, this reversal may be due to a breakdown of the Thomas-Fermi model at low particle densities.

Table I shows representative measured work functions for alleged single crystal planes of tungsten. With the exception of the (110) plane, essentially the same values are measured for each plane. The (110) plane is unusual in that its work function is 0.6 ev to 1.3 ev greater than that of polycrystalline tungsten (≈ 4.6 ev) and at least 0.4 ev greater than the next highest work function plane ($\phi_{211} \approx 4.8$ ev.* Should $\phi_{110} \approx 5.8$ ev, its measurement by thermionic techniques would be almost impossible due to thermal disorder. Because of the extremely good agreement between contact potential difference measurements and field emission measurements, the value $\phi_{110} = 5.9$ ev is used when necessary. To best fit our estimate of $\phi_{110} - \phi_{111} = 1.5$ ev, $F = 0.95$ is used in all subsequent calculations of work function changes due to extremely high applied electric fields. To best fit thermionic data, one should use $F_\sigma \approx 0.3$.

Figures 2 and 3 show the change in work function with applied electric field strength for the (110), (211) (100) and (111) planes of tungsten for field emission and field desorption electric fields, respectively.

For field emission conditions, results are presented for $E \leq 1$ V/Å a value substantially greater than the breakdown field for tungsten ($E \approx 0.7$ V/Å), Although field desorption electric fields can exceed 5 V/Å, the results of this analysis are physically meaningful only up to that strength.

---

* A recent field-electron emission energy distribution measurement yielded $\phi_{110} = 8.78$ ev[2]. However, this result is not confirmed by other researchers as yet.

For $|E| \leq 0.4$ V/Å, $|\delta \phi|$ is approximately the same for both cases and more significantly $|\delta \phi| < 0.2$ ev. Therefore, typical field emission electric fields ($E \approx 0.3$ V/Å) cannot change the work function of any plane of tungsten as measured using thermionic techniques ($\phi_{110} \approx 5.2$ ev) and field emission probe tubes ($\phi_{110} \geq 5.8$ ev).

Figures 4 and 5 show the polarizability of the surface atoms of tungsten on four different planes for both field emission and field desorption electric fields. The polarizabilities increase with field strength for the former because there is no limit to the electronic roughness of the surface. Whereas field desorption fields can produce only an electronically smooth surface with a finite maximum work function decrease that occurs in this formulation for $E \approx 5$ V/Å. The change in charge spreading is negligible here but could be significant for $|E| > 5$ V/Å. Since tungsten field desorbs for $E \approx 5$ V/Å, this effect is of minor significance.

Finally, Figure 6 shows the stress due to a field desorption electric field. At field evaporation $E \approx 5$ V/Å, the stresses are of the same order of magnitude as the tensile strength ($\approx 10^{11}$ dynes/cm^2).

Extremely high electric fields (0.1 V/Å to 10 V/Å) perpendicular to the surface cannot account for the large discrepancies (0.6 ev) between field emission and thermionic emission measured work functions. Those differences appear to be due to thermal rearrangement, patch effects, field emitter flats, misinterpretation of data or other as yet unknown phenomena. The polarizability and stress calculations are important to field emission and field ion microscopy, and similar calculations are planned for surface and kink sites.

References:

1. R. Smoluchowski, Phys. Rev. 60, 661, (1941)

2. R. D. Young and H. E. Clark, Appl. Phys. Letters 9, 265 (1966)

TABLE I

Representative Work Function Values for Clean Single Crystal Planes of Tungsten in Electron Volts.

Plane	Measurement Technique		
	Thermionic	Field Emission	Contact Potential Difference
(110)	5.20	5.9	5.9
(211)	4.78	4.85	-
(100)	4.65	4.72	4.7
(111)	4.30	4.39	4.4

THEORETICAL WORK FUNCTION DIFFERENCES
BETWEEN FOUR PLANES OF TUNGSTEN AS A FUNCTION
OF THE FREE ELECTRON DENSITY

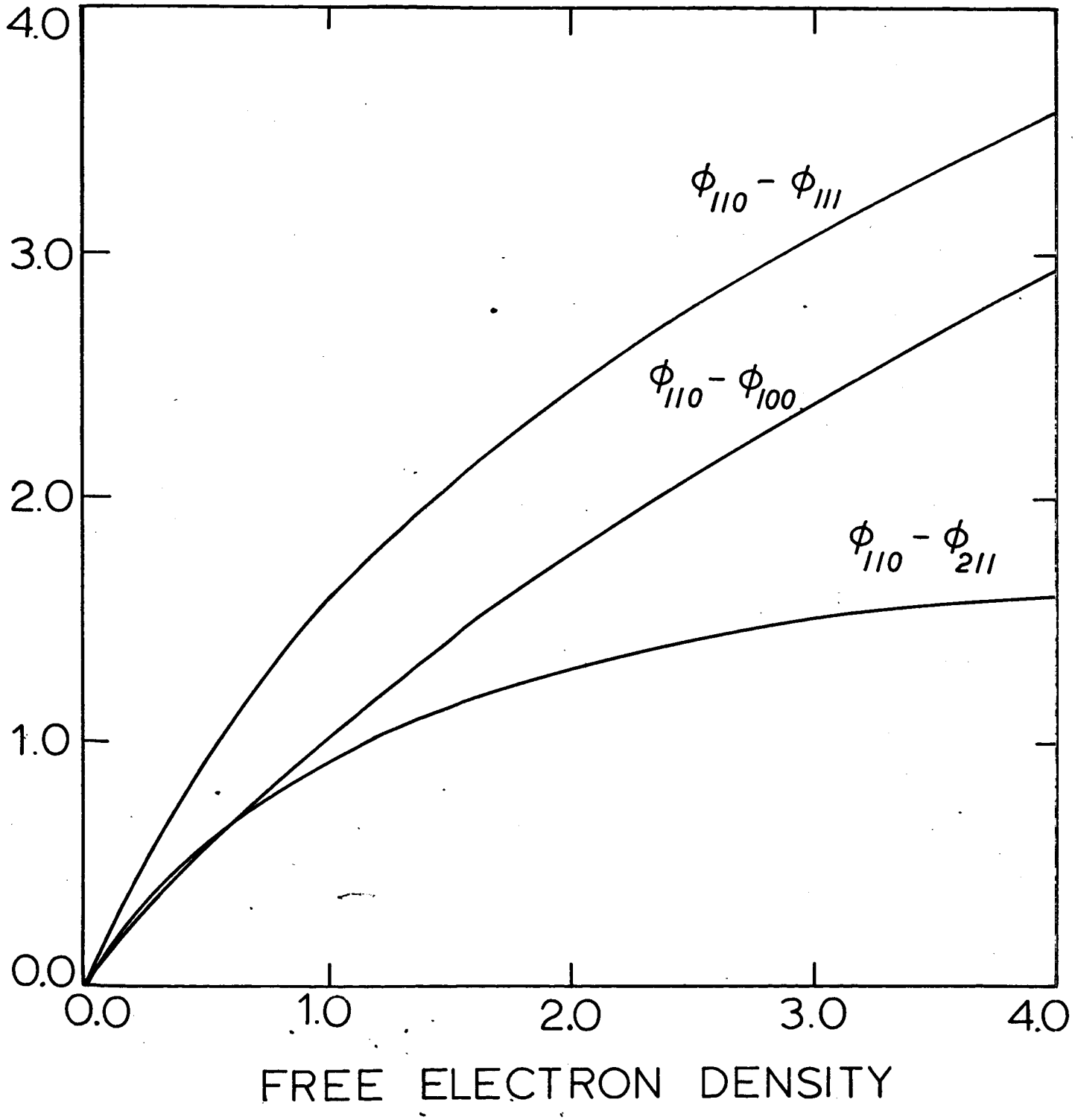

Fig. 1

WORK FUNCTION INCREASES OF FOUR PLANES
OF TUNGSTEN DUE TO A FIELD EMISSION ELECTRIC FIELD

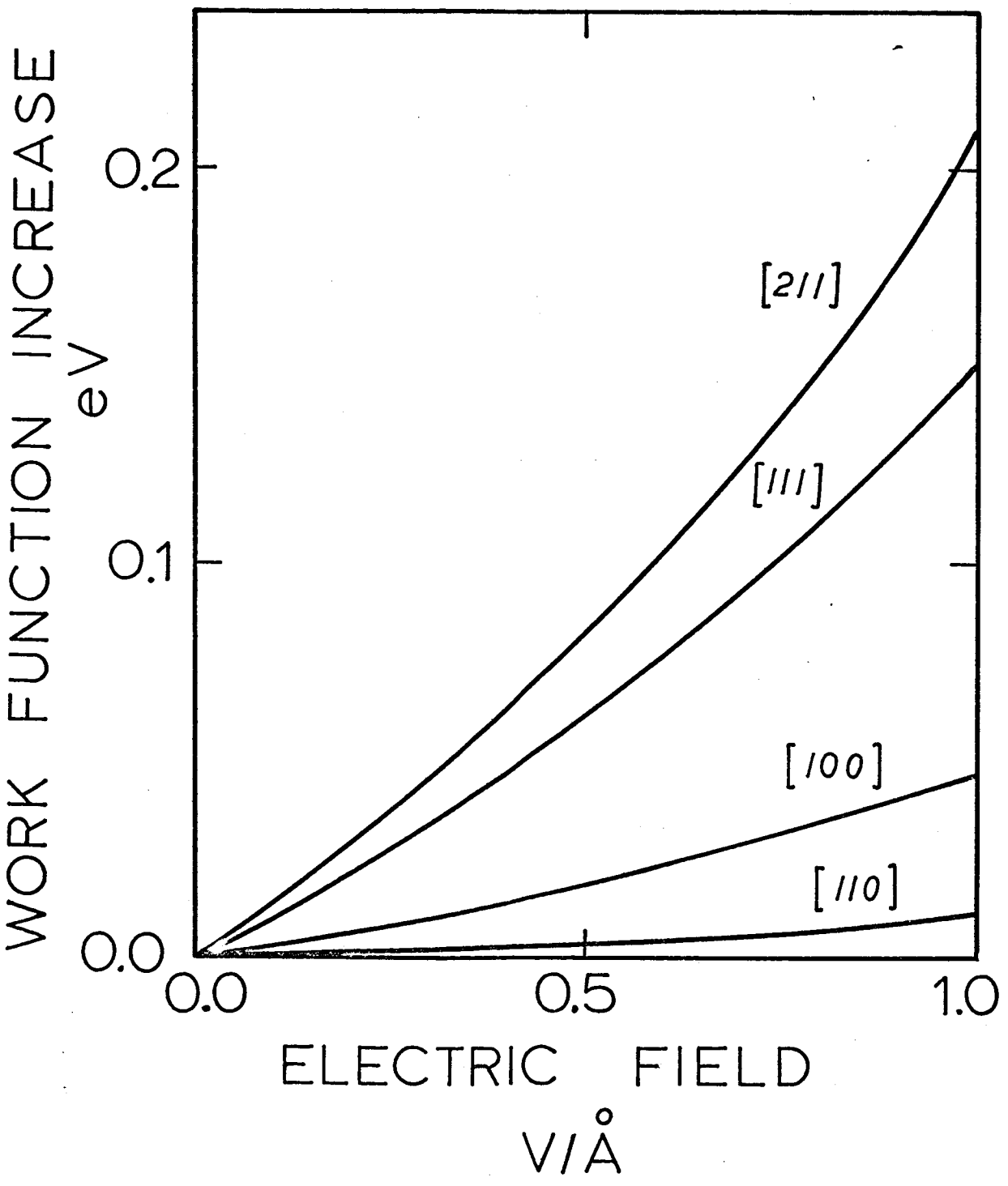

Fig. 2

WORK FUNCTION DECREASES OF FOUR PLANES OF TUNGSTEN
DUE TO A FIELD DESORPTION ELECTRIC FIELD

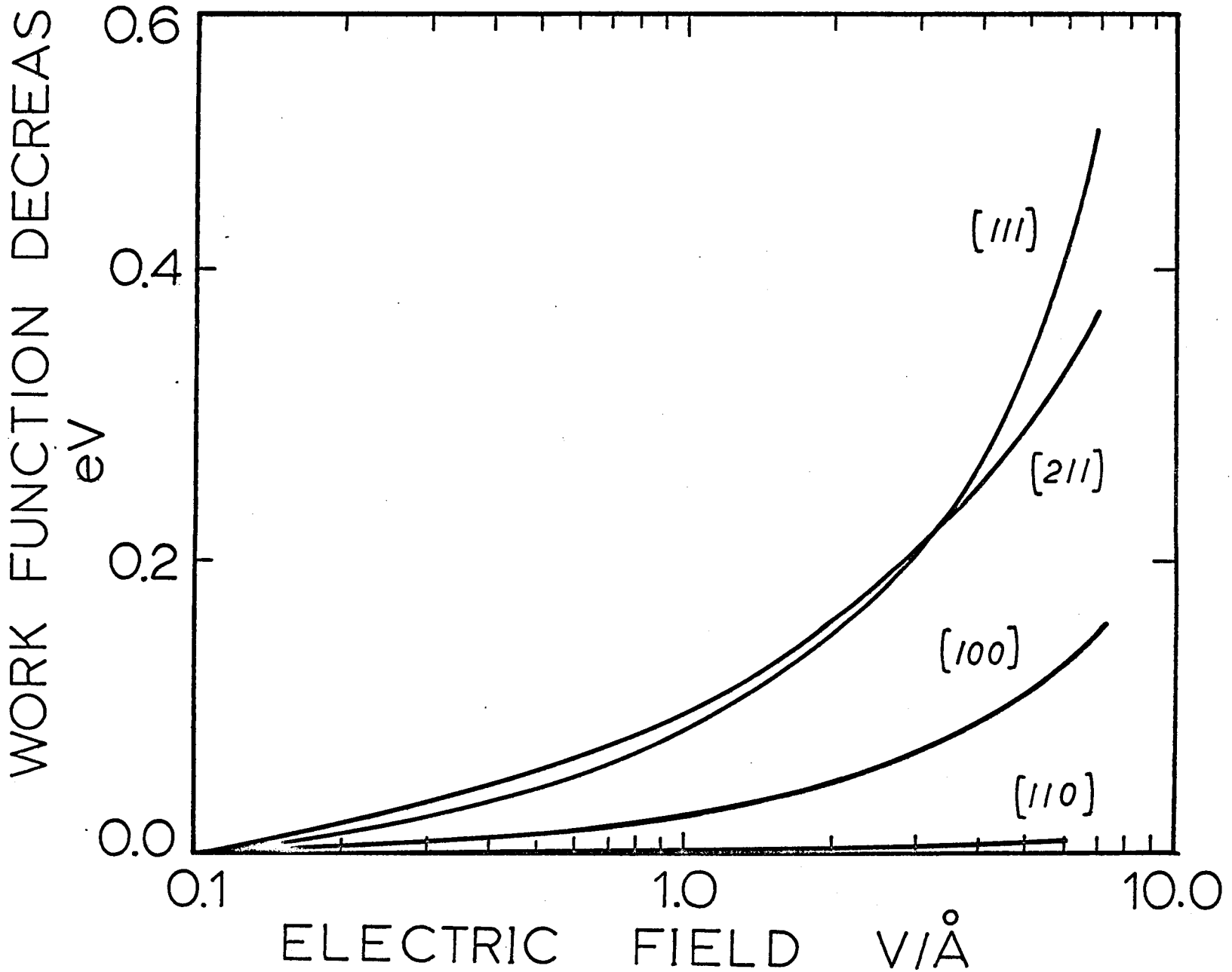

Fig. 3

POLARIZABILITY OF SURFACE ATOMS OF TUNGSTEN
FOR FIELD EMISSION ELECTRIC FIELDS

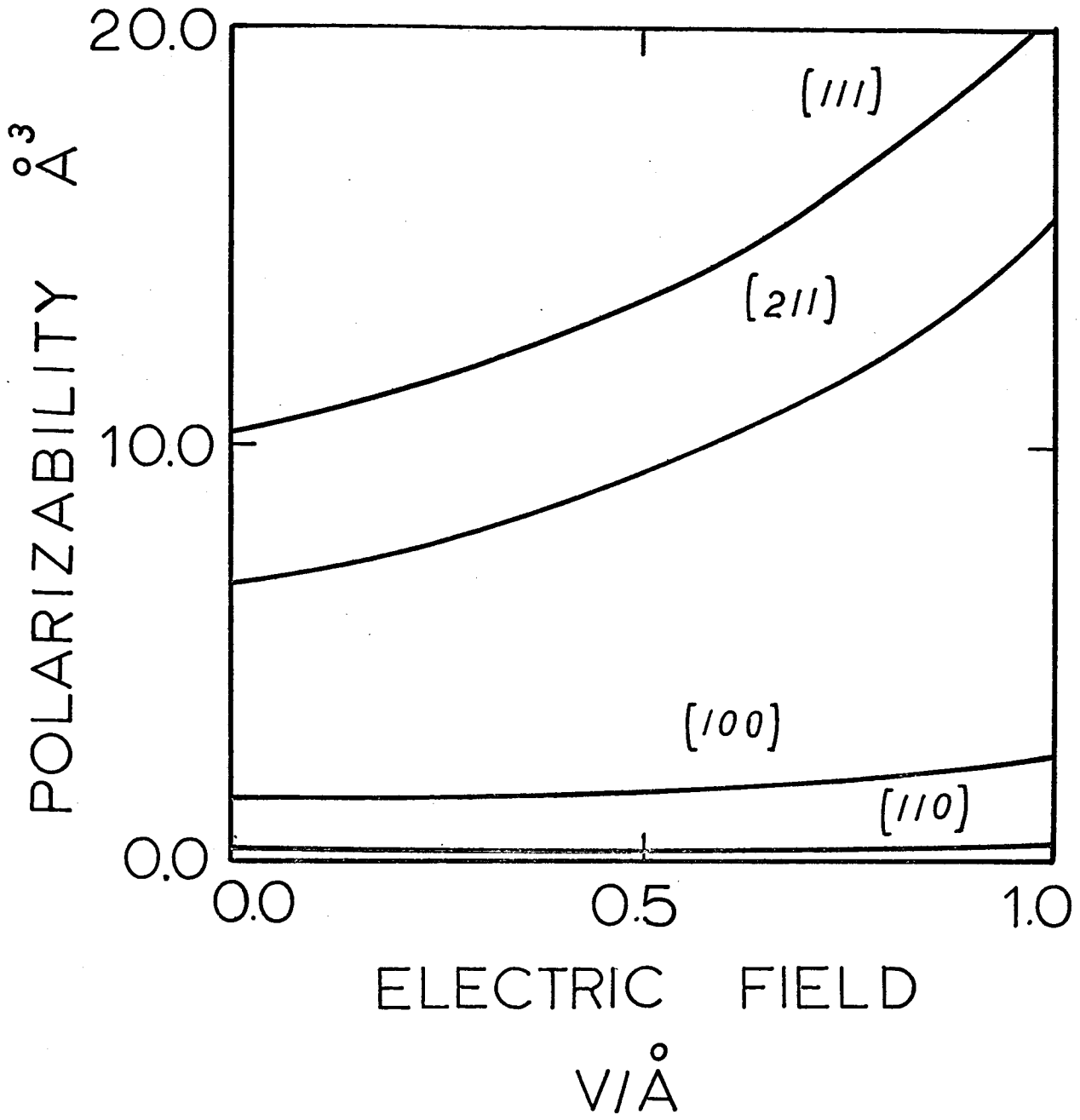

Fig. 4

POLARIZABILITY OF SURFACE ATOMS OF TUNGSTEN
FOR FIELD DESORPTION ELECTRIC FIELDS

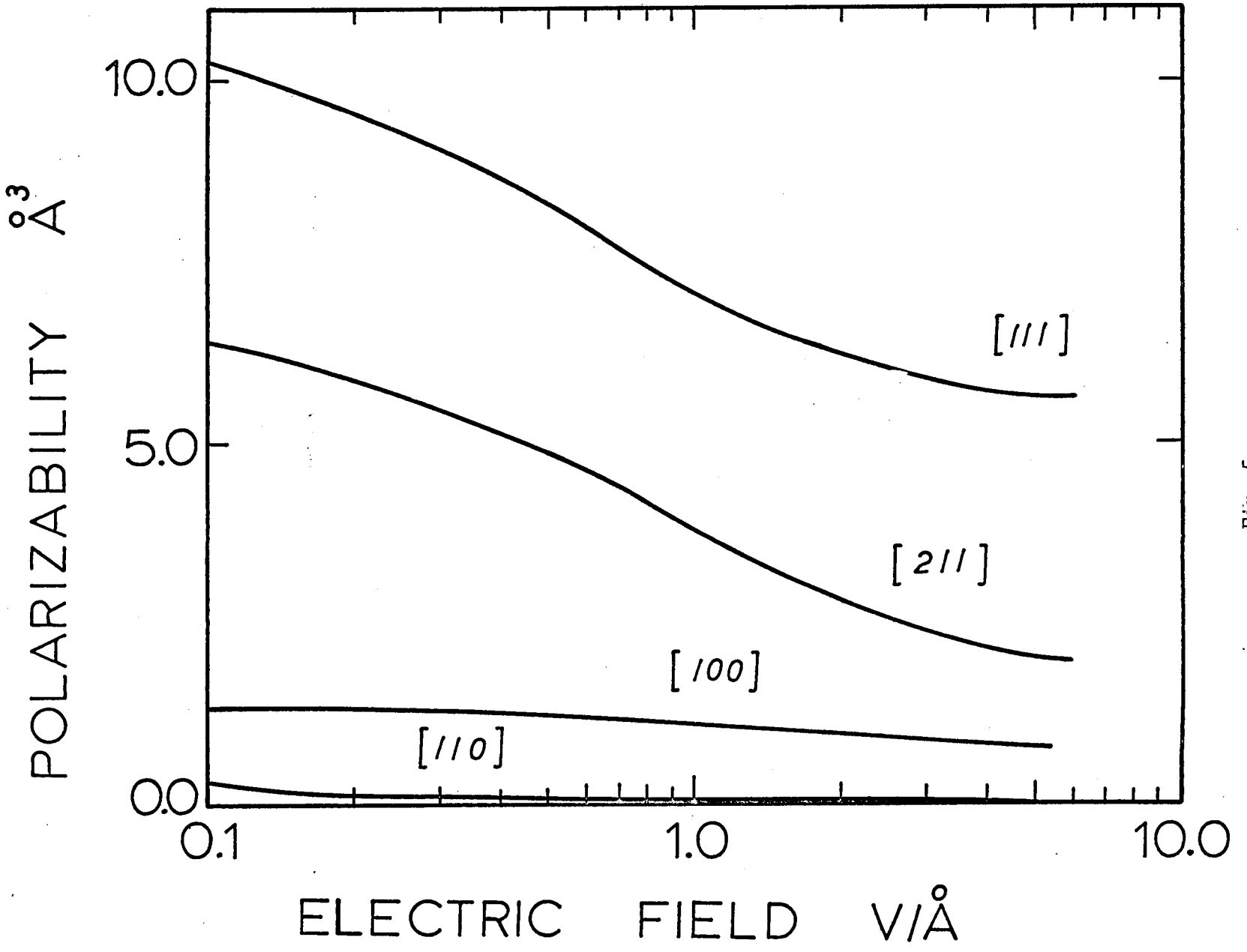

Fig. 5

MECHANICAL STRESS ON FOUR PLANES OF TUNGSTEN
DUE TO FIELD DESORPTION ELECTRIC FIELDS

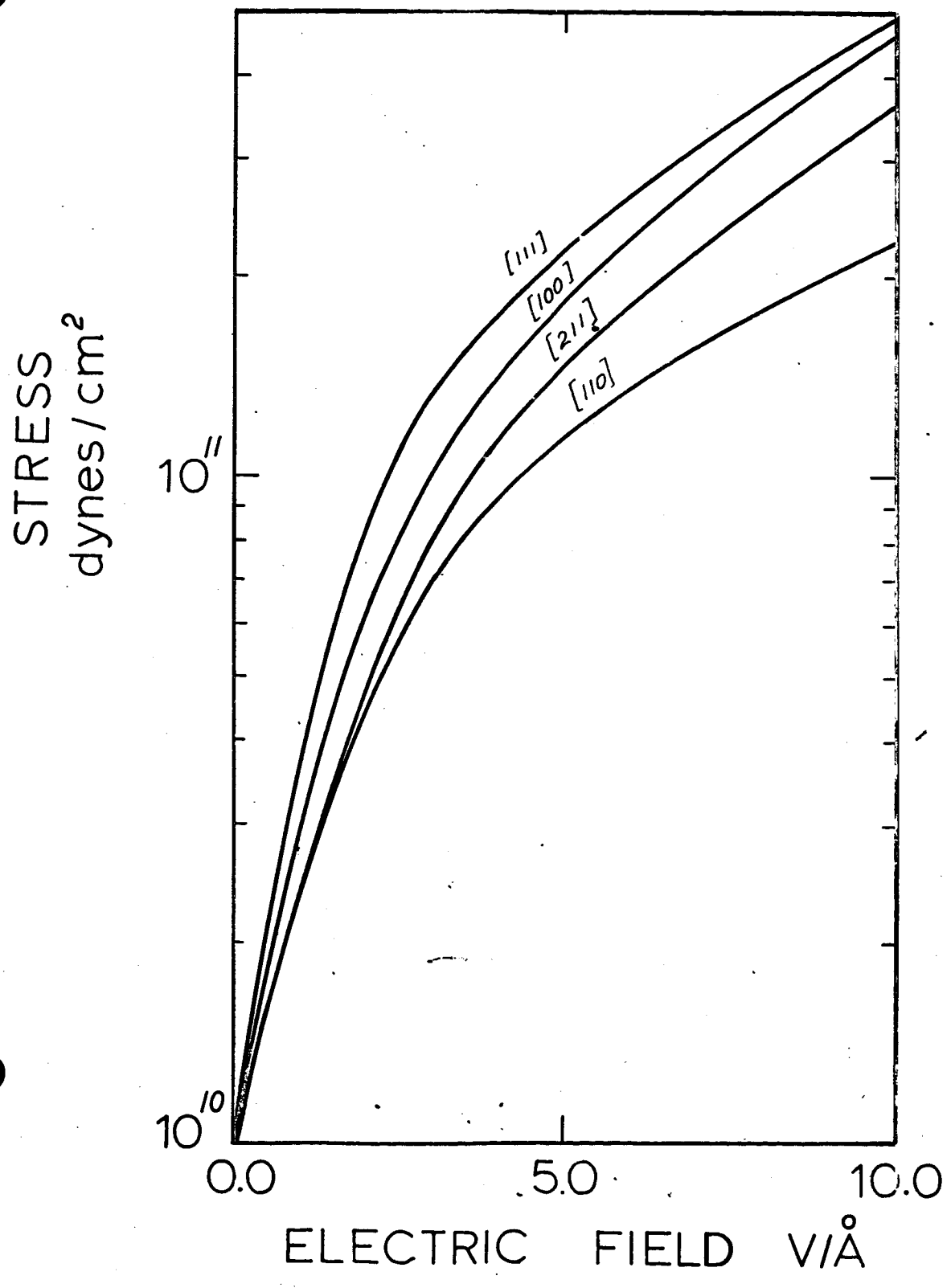

Fig. 6

Thermionic Converters--Characteristics of Thermionic Plasma Diodes with Gas Mixtures

G. L. Schrenk A. Kaufman

The results of these models are currently being studied. Preliminary results indicate that in the ignited mode (and near the maximum power point) negligible improvement can be expected. In the unignited mode, however, sizeable improvements can be expected. The engineering significance of these preliminary findings is currently under study.

ELECTROCHEMICAL ENGINEERING

APPENDIX

A-3

3.1 The Design of Absorption Towers Dissolving H_2 and O_2 in Aqueous KOH

3.1.1 Introduction

Since kinetic limitations of any fuel cell (or electrolytic) system depends on mass transport in the electrolyte, reliance on the porous electrode might be side-stepped entirely. As an alternate type of system, fuel gas could be dissolved into the electrolyte in a gas-liquid contact section and this fuel-enriched liquid could then be passed over electrodes where the appropriate oxidation and reduction reactions take place. Depleted electrolyte could then be recirculated into the contact towers. The arrangement is shown schematically in Fig. 3.1-1.

This report describes the determination of the feasibility of an absorption system integrated with the operation of a fuel cell. The absorption system saturates a 4N KOH electrolyte solution with oxygen and hydrogen, and this study evaluates the size flow and power consumption characteristics of the towers. Coupled with assumptions that are reasonable for a 200 watt fuel cell operating at 20°C, tower heights at 3.6 ft for H_2 column and 5.1 ft for the O_2 column with one square foot cross sectional area are indicated. Pumping losses are estimated to be 26% of the available power, thus indicating borderline feasibility. Note, however, that the design specifications were arbitrarily chosen, and, with slight modifications, the system can be shown to be completely feasible, i.e., optimization can be readily accomplished.

3.1.2 Design Assumptions

The following assumptions were made when designing the absorption system. These assumptions apply to both the H_2 and O_2 towers.

a. A packed tower is the most efficient method, in terms of tower volume, for absorbing a gas in a liquid on a small scale, i.e., to supply the needs of a 200 W fuel cell.

b. Steady state transfer of gas into the liquid stream.

c. Pure gas is being fed into the bottom of the tower.

d. Pure liquid is being fed into the top of the tower.

e. The liquid film is the principle resistance to diffusion, and, therefore, the liquid at the interface may be assumed to be in equilibrium with the main body of the gas.

f. The gas and liquid phases pass counter-current to each other.

g. The liquid is non-volatile.

h. The volumetric flow rate of gas through the tower remains constant.

i. The density of the liquid throughout the tower is constant.

j. The operation takes place in the presence of gravity ($g = 32.2$ ft/sec^2).

k. The amount of gas dissolved in the electrolyte at a particular pressure can be expressed by a Henry's law constant because of the low gas concentrations involved.

l. The fuel cell converts 50% of the available chemical energy into electrical energy.

m. No flooding is to occur in any section of the column.

n. The column operates isothermally.

o. The viscosity of the liquid throughout the column is constant.

p. The diffusion coefficient of the liquid throughout the column is constant since it can be shown that the concentration of dissolved gas is very small throughout the length of the column.

3.1.2.1 Design Specifications

All calculations in this report will be based on the following design specifications. They are believed to be reasonable values for possible operating conditions.

a. The temperature of the columns is 25°C.

b. The pressure of the incoming gas to the columns is 5 atm.

c. The cross sectional area of the columns is one square foot.

d. The fuel cell is producing 200 watts of electrical energy.

e. The towers will be packed with stoneware Raschig rings[6] whose diameter and height equal one inch and whose wall thickness equals 3/32 inch.

f. The concentration of the gas in the electrolyte at the bottom of both columns will be specified to be in equilibrium with a pressure of 3 atmospheres of the pure gas.

3.1.2.2 Design Variables

The following design parameters will be calculated for each column.

a. The pressure of the gas effluent at the top of the column.

b. The concentration of the dissolved gas in the liquid effluent.

c. The molar gas flow rate per unit cross sectional area.

d. The mass gas flow rate per unit cross sectional area.

e. The volumetric gas flow rate per unit cross sectional area.

f. The molar liquid flow rate per unit cross sectional area.

g. The mass liquid flow rate per unit cross sectional area.

h. The volumetric liquid flow rate per unit cross sectional area.

i. The height of the columns.

j. The volume of the columns.

k. The volume of the columns occupied by gas.

l. The volume of the columns occupied by liquid.

m. The contact time of the liquid.

n. The contact time of the gas.

o. The moles of gas absorbed per hour and fed to the fuel cell.

A table of the calculated values of these parameters is presented in Section 3.1.8.

3.1.3 Derivation of the Design Equations

3.1.3.1 Mass Transfer

Restricting the design to steady state transfer of a solute from a gas stream to a liquid stream, it is evident that all solute diffusing from gas to interface must diffuse at the same rate from the interface to the main body of liquid, hence

$$N = k_g (P-P_i) = k_l (c_i - c) \qquad 3.1\text{-}1$$

N = rate of mass transfer, lb mole/hr ft^2.

P = partial pressure of diffusing gas in the main stream, atm.

c = bulk concentration, lb mole/ft^3.

P_i = partial pressure of diffusing gas at the phase boundary, atm.

c_i = concentration at the phase boundary, lb mole/ft^3.

k_g = individual or gas-film coefficient, lb mole/hr ft^2 atm.

k_l = individual or liquid-film coefficient, lb mole/hr ft^2, lb mole ft^{-3}.

Equation 1 has little practical utility since it is necessary to know both k_g and k_l as well as the equilibrium relation between P_i and c_i in order to calculate N. It is convenient, therefore, to employ overall coefficients K_l and K_g which may be used to calculate N without knowledge of c_i or P_i.

$$N = K_g (P - P_e) = K_l (c_e - c) \qquad 3.1\text{-}2$$

K_g = overall mass transfer coefficient, lb mole/hr ft^2 atm.

K_l = overall mass transfer coefficient, lb mole/hr ft^2 lb mole ft^{-3}.

P_e = partial pressure of the solute over a solution having the composition of the main liquid stream, c, atm.

c_e = concentration of a solution in equilibrium with the solute partial pressure, P, lb mole/ft^3.

Thus, $P - P_e$ is the overall driving force expressed in partial pressure units, and $c_e - c$ is the overall driving force expressed in concentration units. The overall coefficients K_g and K_l have great utility, and most experimental studies of mass transfer between phases give information as to K_g or K_l, but not k_g or k_l.

For the present system, O_2 and H_2 absorption in KOH, it will be assumed that the liquid film offers the principal resistance to diffusion, and, therefore, the liquid at the interface may be assumed to be in equilibrium with the main body of the gas, i.e., $c_i = c_e$. The driving force is, therefore, the difference between the concentrations, c_e and c, obtained from the equilibrium and operating lines respectively, at any partial pressure, P, in the main body of the gas.

Since $c_i = c_e$, substitution in Equation 3.1-1 yields

$$N = k_l (c_e - c) \qquad 3.1\text{-}3$$

But from Equation 3.1-2, it is evident that $N = K_l (c_e - c)$, so that for our particular system,

$$k_l = K_l \qquad 3.1\text{-}4$$

For a packed tower, the following is true:

$$(N)(a)(dV) = k_l (a)(c_e - c)\, dv \qquad 3.1\text{-}5$$

a = interfacial area per unit volume, a function of the type of packing being used, ft^2/ft^3.

Now consider the gas liquid contact process to consist of counter-current absorption of pure gas into liquid KOH. The absorbent enters at the top of the tower containing L_M lb moles per hour of solute free non-volatile liquid per square foot of tower cross section. In passing through to the lower end of the tower, the solute concentration in the absorbent increases to X_B lb moles of solute per lb mole of absorbent. X_B equals some fraction of X_{eB} corresponds to a composition, which is in equilibrium with the solute partial pressure at the bottom of the column.

The gas to be treated is pure and it enters at the bottom of the column at the rate G_{MB} lb mole per hr ft^2. In designing the column, it is assumed that the volumetric flow rate of the gas remains constant. This condition dictates a pressure drop along the length of the column proportional to gas absorption as:

$$P_B - P_r = \Delta n \frac{RT}{V_g} = \frac{(G_{MB} - G_{MT})(RT)(t_g A)}{(V_g)} \qquad 3.1\text{-}6$$

P_B = pressure of pure gas at the bottom of the column, atm.

P_T = pressure of pure gas at the top of the column, atm.

G_{MB} = molar flow rate of gas at the bottom of the column, lb mole/hr ft^2.

G_{MT} = molar flow rate of gas at the top of the column, lb mole/hr ft^2.

Δn = moles absorbed, moles.

T = temperature of column, ^oR.

R = gas constant, ft^3 atm/^oR lb mole .

V_g = the volume occupied by the gas in the column, ft^3.

A = cross sectional area of the column, ft^2.

t_g = contact time of the gas in the column, hr.

Note also that $d t_g / d V_g$ is constant throughout the column and is equal to t_g / V_g.

Let

$$\frac{RT\ t_g\ A}{V_g} = \text{constant} = \Omega$$

$$P_B - P_T = \Omega\ (G_{MB} - G_{MT}) \qquad 3.1\text{-}6a$$

Equation 3.1-6a can be applied to any point in the column so that

$$P_B - P = \Omega\ (G_{MB} - G_M) \qquad 3.1\text{-}7$$

$$P - P_B = \left(\frac{P_B - P_T}{G_{MB} - G_{MT}}\right)(G_M - G_{MB}) \qquad 3.1\text{-}7a$$

$$P = \left(\frac{P_B - P_T}{G_{MB} - G_{MT}}\right)\ G_M + \left[P_B - G_{MB}\left(\frac{P_B - P_T}{G_{MB} - G_{MT}}\right)\right] \qquad 3.1\text{-}8$$

Equation 3.1-8 clearly shows the linear dependence of P on G_M and can be used to calculate P at any point. For the top and bottom of the column, P_T and P_B can be calculated from Equation 3.1-6a.

Design considers the impossibility of absorbing all the gas since that would mean that G_{MT} must equal zero and, correspondingly, $P_T = 0$. This is an undesirable situation and, clearly, the value of G_{MT} must be compromised to yield some finite value.

3.1.3.2 Material Balance

An overall material balance around the column can be written as follows:

$$(L_M)\ (X_B) = G_{MB} - G_{MT} \qquad 3.1\text{-}9$$

Similarly at any point in the column

$$(L_M)\ (X_B - X) = G_{MB} - G_M \qquad 3.1\text{-}10$$

$$(L_M)\ dX = d\,G_M \qquad 3.1\text{-}11$$

or

$$(L/\rho)\ dc = d\,G_M = L_M\ dX \qquad 3.1\text{-}11a$$

L = mass flow rate per unit area, lb/hr ft^2.

ρ = density of the liquid, lb/ft^3.

Combining Equation 3.1-11 with the diffusional relation, Equation 3.1-5, there is obtained

$$L_M\,dX = (K_l)\ (a)\ (c_e - c)\ (dV/h) \qquad 3.1\text{-}12$$

$$L_M\,dX = (K_l)\ (a)\ (c_e - c)\ (dh) \qquad 3.1\text{-}12a$$

dh = differential tower height, ft.

Integrating Equation 3.1-12a gives

$$h = L_M \int_{X_T}^{X_B} \frac{dX}{K_l\ a\ (c_e - c)} \qquad 3.1\text{-}13$$

Substituting Equation 3.1-11a into Equation 3.1-13 gives

$$h = \frac{L}{\rho} \int_{c_T}^{c_B} \frac{dc}{K_l\ a\ (c_e - c)} \qquad 3.1\text{-}14$$

Since c_T is specified to be pure depleted solvent,

$$h = L/(\rho a)\int_0^{c_B} \frac{dc}{K_l (c_e - c)} \qquad 3.1\text{-}15$$

3.1.3.3 Tower Design Correlations

In order to evaluate Equation 3.1-15, a knowledge of K_l is needed since $\underline{a}$ can be obtained from the literature for the particular packing being considered. Since no theoretical model has yet proved adequate[1] to predict absorption rates in packed columns, empirical correlations are recommended. One such correlation that adequately describes a great number of systems was proposed by Van Krevelen and Hoftijer[2,3].

$$\frac{K_l (\mu^2/\rho^2 g)^{1/3}}{D} = .015\,(Re)^{2/3}\,(Sc)^{1/3} = .015\left(\frac{L}{\bar{a}\,\mu}\right)^{2/3}\left(\frac{\mu}{\rho\,D}\right)^{1/3} \qquad 3.1\text{-}16$$

and $\bar{a}/a = 1 - e^{-.4L/\rho}$ 3.1-16a

ρ = density of the solution, lb/ft^3.

μ = viscosity of the solution, lb/ft hr.

D = diffusion coefficient of the gas in the solution, ft^2/hr.

g = gravitational constant, ft/hr^2.

$\bar{a}$ = effective interfacial area of packing, ft^2/ft^3.

a = theoretical interfacial area of packing, ft^2/ft^3.

Rearranging Equation 3.1-16 in terms of K_l and substituting for $\bar{a}$, there is obtained

$$K_l = .015\left[\frac{L}{(1-e^{-.4L/\rho})\,a}\right]^{2/3}\left(\frac{1}{\mu}\right)(g)^{1/3}\,(\rho)^{1/3}\,(D)^{2/3}$$

3.1-17

If it is assumed that all physical parameters remain constant in the column, utilizing Equation 3.1-17 in Equation 3.1-15 and taking the constant parameters outside the integral, one gets the very important result,

$$h = (66.7)\left(\frac{L}{a\,g}\right)^{1/3}(\mu)\,(\rho^{-4/3})\,(1-e^{-4L/\rho})^{2/3}(D)^{-2/3}\int_0^{c_B}\frac{dc}{c_e - c}$$

3.1-18

Obviously to solve Equation 3.1-18 for the tower height, one needs experimental data giving c_e as a function of c. Note, however, that literature data can be utilized to give $c_e = f(P)$ (saturation concentration as a function of the partial pressure above it), but by employing Equations 3.1-8, 3.1-11a), this data can be converted to give c_e as a function of c.

3.1.3.4 Flow Rate, Liquid

One parameter is still undefined in Equation 3.1-18, and it must be evaluated before the tower height can be calculated, and this parameter is L.

At this point, it should be observed that the bottoms of the absorption towers is being fed into a fuel cell. The amount of dissolved gas coming out of the towers is then fixed by the power requirements of the cell.

For instance, in this problem, it is specified that the electrical output of the cell is 200 watts. Therefore, in one hour, it will produce an energy equal to 200 watt hours.

.2 Kwatt hrs x 2.65 x 10^6 ft lb/Kwatt hr x .324 cal/ft lb x 1 Kcal/1000 cal = 170 Kcal

Now if one assumes a 50% conversion of chemical energy (free energy of formation) to electrical energy, then 340 Kcal of chemical energy must be produced. Allowance is thus made for overvoltage and resistive losses on a crude estimate basis.

We know that the reaction $H_2 + 1/2\ O_2 \rightarrow H_2O$ (25°C/1 atm) produces 57 Kcal/g mole of H_2O. Therefore, 6 g mole of water will have to be produced in order to meet the power requirement.

If it is assumed that all oxygen and hydrogen fed into the fuel cell is consumed, i.e., completely reacted, then 6 g mol per hour of H_2 are necessary, .0132 lb mole H_2/hr, and 3 g mol per hour of O_2 are necessary, .0066 lb mole O_2/hr.

Therefore, the liquid flow rate of the O_2 tower is equal to

$$L = (.0066)/(c_B)\ (A)\ (1/\rho) \qquad 3.1\text{-}19$$

and the liquid flow rate of the H_2 tower is

$$L = (.0132)/(c_B)\ (A)\ (1/\rho) \qquad 3.1\text{-}20$$

Note that the cross sectional area of both towers is arbitrarily specified at 1 ft^2, and the tower height can be readily calculated using Equation 3.1-18.

3.1.3.5 Contact Times

One can now go about determining t_g and t_l, the contact times of the vapor and liquid in the tower. In obtaining the contact time of the vapor, it is assumed that the vapor of the inlet is at a pressure of 5 atmospheres and ϵ designates the void volume coefficient.

$$t_g = V_g / \bar{V}A \qquad 3.1\text{-}21$$

V_g = volume of tower available for vapor flow, ft^3.

$\bar{V}$ = volumetric gas rate, ft^3/ft^2 hr.

$$V_g = V\epsilon \frac{V_g}{V_g + V_l} \qquad 3.1\text{-}22$$

V_g and V_l are also proportional to the volumetric flow rates of the gas and liquid respectively, therefore,

$$V_g = V\epsilon \frac{\bar{V}}{\bar{V} + \overset{x}{V}} \qquad 3.1\text{-}23$$

$\overset{x}{V}$ = volumetric liquid rate, ft^3/ft^2hr.

But $$\bar{V} = 77 \times G_{MB} \qquad 3.1\text{-}24$$

$$\overset{x}{V} = L/\rho \qquad 3.1\text{-}24a$$

Therefore, substituting Equation 3.1-24, 3.1-24a in Equation 3.1-23 and placing Equation 3.1-23 in Equation 3.1-21, we obtain

$$t_g = \frac{V\epsilon}{A(77 \times G_{MB} + L/\rho)} \qquad 3.1\text{-}25$$

But

$$V = hA \qquad 3.1\text{-}26$$

Therefore,

$$t_g = \frac{h\epsilon}{77\, G_{MB} + L/\rho} \qquad 3.1\text{-}27$$

It is also obvious that

$$V_g = V\epsilon \frac{77 \times G_{MB}}{77 \times G_{MB} + L/\rho} \qquad 3.1\text{-}28$$

Similarly, the contact time of the liquid in the tower is

$$t_l = \frac{h\epsilon}{77 \times G_{MB} + L/\rho} \qquad 3.1\text{-}29$$

and the volume of the tower occupied by the liquid is

$$V_l = V\epsilon \quad \frac{L/\rho}{77 \times G_{MB} + L/\rho} \qquad 3.1\text{-}30$$

3.1.3.6 Flooding Limits

All of the preceding five equations, 3.1-25, 27, 28, 29, 30, necessitate a knowledge of G_{MB}, the molar gas flow rate coming into the bottom of the column. This parameter can be obtained by considering flooding requirements dictated by the specific tower[10].

The flooding rate can be calculated from the following equation.

$$\ln \frac{G_f^2 \, a\mu_l^{-2}}{g\epsilon^3 \rho_g \rho_l \mu_w^{-2}} = -4 \left(\frac{L}{G}\right)^{1/4} \left(\frac{\rho_g}{\rho_l}\right)^{1/8} \qquad 3.1\text{-}31$$

G_f = flooding rate expressed as mass flow of the gas phase per unit area of column cross-section, $lb/ft^2 sec$

g = acceleration due to gravity, ft/sec^2

G = mass flow rate of gas phase, $lb/hr\ ft^2$

L = mass flow rate of liquid phase, $lb/hr\ ft^2$

μ_w = viscosity of water, $lb_m\ ft^{-1}\ hr^{-1}$

The usual technique is to allow G to equal 60 to 80% of the flooding rate; therefore Eq. 3.1-31 can be rewritten in terms of G_f only as

$$\ln \frac{G_f^2 \ (a) \ \mu_l^{-2}}{(g) \ (\epsilon)^3 \ (\rho_g) \ (\rho_l) \ \mu_w^{-2}} = -4 \left(\frac{L}{Z \ 3600 \ G_f}\right)^{1/4} \left(\frac{\rho_g}{\rho_l}\right)^{1/8}$$

3.1-32

where Z is some coefficient ranging between .6 and .8 . Obviously then

$$G_{MB} = (Z)(3600)(G_f)/MW_g \qquad 3.1\text{-}33$$

The equations derived and enumerated in Section 3.1.3 are sufficient to calculate all column parameters, and this will be demonstrated in Section 3.1.5. However before any column calculations are performed, some physical properties of the system will be given.

3.1.4 Physical Data

3.1.4.1 Physical data pertaining to both the O_2 and H_2 absorption towers

a) Viscosity of 4N KOH[4] at 18°C

μ = 1.54 c.p. = 3.74 $lb_m/ft\ hr$

b) Density of 4N KOH at 20°C[5]

ρ_l = 1.18 g/ml = 73.5 lb/ft^3

c) MW of 4N KOH at 20°C

$MW_l = \rho(18) = (1.18)(18) = 21$ lb/lb mole

d) The towers will be randomly packed with stoneware Raschig rings[6] whose diameter and height equal 1 inch and whose wall thickness equals 3/32 inch

ϵ = 68%

a = 58 ft^2/ft^3

3.1.4.2 Physical data pertaining specifically to the O_2 tower

a) the diffusion coefficient of O_2 in 4N KOH, 20% by weight KOH, at 25°C, and extremely dilute O_2 content,[7] is

$$D = 10^{-5}\ cm^2/sec = 3.9 \times 10^{-5}\ ft^2/hr$$

b) In order to generate solubility data for O_2 in 4N KOH, it will be assumed that a Henry's law constant applies throughout the length of the column. Therefore $X_{O_2} = P/H_{O_2}$ (X is the mole fraction of O_2 dissolved P is the pressure above the solution, and H_{O_2} is the Henry's Law constant). Using the data of Gubbins and Walker,[7] the solubility of O_2 at a pressure of one atmosphere in 4N KOH, 20% by wt. KOH, at 25°C is $.25 \times 10^{-3}$ g mole/liter.

$$X_{O_2} = \frac{.25 \times 10^{-3}}{55} = 4.6 \times 10^{-6} \qquad \text{and therefore}$$

$$H_{O_2} = P/X_{O_2} = 1/4.6 \times 10^{-6} = 2.2 \times 10^{5}\ \frac{atm}{\text{mole fraction}} \qquad 3.1\text{-}34$$

c) ρ_g, the density of the oxygen gas at 70°F and 5atm is, utilizing the perfect gas law, .41 lb/ft^3 .

3.1.4.3 Physical data pertaining specifically to the H_2 tower.

a) No information could be found regarding the diffusion coefficient of H_2 in a 4N KOH solution, however the following assumption will be utilized.

$$\frac{D_{H_2} \text{ in pure water}}{D_{H_2} \text{ in 4N KOH}} = \frac{D_{O_2} \text{ in pure water}}{D_{O_2} \text{ in 4N KOH}}$$

D_{H_2} in pure water = 5.85×10^{-5} cm^2/sec [8]

D_{O_2} in pure water = 1.9×10^{-5} cm^2/sec [7]

D_{O_2} in 4N KOH = 10^{-5} cm^2/sec [7]

Therefore, D_{H_2} in 4N KOH equals 3.1×10^{-5} cm^2/sec or 12×10^{-5} ft^2/hr

b) Geffken[11] shows that the ratio of the solubility of H_2 in 4N KOH to H_2 in pure water, at 25^oC is 0.3 .

Therefore

H_{H_2} in 4N KOH = $\frac{1}{.3}$ H_{H_2} in pure water

H_{H_2} in pure water = 7.5×10^4 atm/mole fraction[9], so

H_{H_2} in 4N KOH = 25×10^4 atm/mole fraction

c) The density, ρ_g of the hydrogen at 70^oF and 5atm is utilizing the perfect gas law, .026 lb/ft^3 .

3.1.5 Design of the O_2 Tower

The first step in the design of the O_2 tower is to calculate the liquid flow rate, L , based on the fuel needs of the electrochemical cell. Eq. (19) will be utilized.

$A = 1\ ft^2$

$\rho_l = 73.5\ lb/ft^3$

To solve Eq. (19) one must also have knowledge of c_B , the concentration of O_2 dissolved in the effluent solvent. Referring to Eq. (34)

$X_B = P/H$

and for dilute solutions it can easily be shown that

$$X = (c)(MW_1)/\rho_1 \qquad 3.1\text{-}35$$

Substituting Eq. (35) in Eq. (34) gives

$$c = (P)(\rho_1)/(H)(MW_1) \qquad 3.1.36$$

P = the pressure with which the dissolved gas is in equilibrium, since the effluent concentration is specified to be in equilibrium with a pressure of 3 atm , P = 3 atm.

MW_1 = 21 lb/lb mole

H_{O_2} = 2.2×10^5 atm/mole fraction

c_B is calculated to be 4.8×10^{-5} lb mole/ft^3

L is calculated to be 10,200 lb/hr ft^2

L_M is calculated to be 482 lb mole/hr ft^2

Referring to Eq. (9)

$$X_B = 1.36 \times 10^{-5}$$

$$L_M = 482 \text{ lb/hr ft}^2$$

$$(X_B)(L_M) = 6.6 \times 10^{-3} \quad \frac{\text{lb mole}}{\text{ft}^2 \text{ hr}}$$

What immediately becomes apparent is that if $G_{MB} >> 1 \frac{\text{lb mole}}{\text{hr ft}^2}$, then G_{MT} approximately equals G_{MB}. One can calculate G_{MB} from Eq. (32) and Eq. (33).

$a = 58\ ft^2/ft^3$ $\qquad MW_g = 32$

$\mu_l = 1.54$ c.p. at 20^oC

$\mu_w = 1.06$ c.p. at 20^oC

$g = 32.2\ ft/sec^2$

$\epsilon = .68$

$\rho_g = .41\ lb/ft^3$

$\rho_l = 73.5\ lb/ft^3$

$Z = .6$

Solving Eq. (32) for G_f yields $.25\ lb/ft^2$ sec

Solving Eq. (33) for G_{MB} yields 16.9 lb moles of O_2/ft^2 hr

G_B is calculated to be $540\ lb/hr\ ft^2$

Indeed it is evident that $G_{MB} >> 1\ \frac{lb\ mole}{hr\ ft^2}$, therefore $G_{MB} \approx G_{MT} \approx G_M \approx$ 16.9 lb moles of $O_2/hr\ ft^2$. Referring to Eq. (8) a necessary consequence of the preceding statement is that $P_B \approx P_T \approx P \approx 5$ atm.

One can now utilize Eq. (18) to calculate the height of the tower. Note that the assumption concerning the constant pressure throughout the length of the column considerably simplifies the integration since c_e is merely taken to be constant throughout the column.

c_e is calculated using Eq. (36) with P equal to 5atm. c_e equals 8×10^{-5} lb mole/ft^3.

Substituting appropriate values for constants in Eq. (18)

$L = 10{,}200\ lb/hr\ ft^2$ $\qquad D = 3.9 \times 10^{-5}\ ft^2/hr$

$a = 58\ ft^2/ft^3$ $\qquad c_e = 8 \times 10^{-5}$ lb mole/ft^3

$g = 2.5 \times 10^{-6}\ ft/hr^2$ $\qquad c_B = 4.8 \times 10^{-5}$ lb mole/ft^3

$\mu = 3.74\ lb_M/ft\ hr$

$\rho = 73.5\ lb/ft^3$

h comes out to be 5.1 ft.

Referring to Eq. 3.1-26, $V = 5.1\ ft^3$

" " Eq. 3.1-28, where $\epsilon = .68$, $V_g = 3.14\ ft^3$

" " Eq. 3.1-27, $t_g = 2.4 \times 10^{-3}$ hr

" " Eq. 3.1-30, $V_l = .33\ ft^3$

" " Eq. 3.1-29, $t_l = 2.4 \times 10^{-3}$ hr

3.1.6 Design of the H_2 Tower

The first step in the design of the H_2 tower is to calculate the liquid flow rate, based on the fuel needs of the electrochemical cell. Eq. 3.1-20 will be utilized. However, in order to solve Eq. 3.1-20 one must also have knowledge of c_B, the concentration of H_2 dissolved in the effluent solvent. Referring to Eq. 3.1-34

$P = 3$ atm

$\rho_l = 73.5\ lb/ft^3$

$MW_l = 21\ lb/ft^3$

$H_{H_2} = 2.5 \times 10^5$ atm/mole fraction

Referring to Eq. 3.1-34, c_B equals 4.2×10^{-5} lb mole/ft^3

" " Eq. 3.1-20, L equals 23,000 lb/hr ft^2

L_M is calculated to be 1100 lb mole solvent/hr ft^2

Referring to Eq. 3.1-9

$X_B = 1.2 \times 10^{-5}$

$L_M = 1100$ lb mole/hr ft^2

$(X_B)(L_M) = 1.32 \times 10^{-2}$ lb mole/ft^2 hr

What immediately becomes apparent is that if

$G_{MB} >> 1 \frac{\text{lb mole}}{\text{hr ft}^2}$, then G_{MT} approximately equals G_{MB}. One can

One can calculate G_{MB} from Eq. 3.1-32 and Eq. 3.1-33. All constants are the same as those employed in the design of the O_2 tower except that

$Z = .8$

$L = 23{,}000$ lb/hr ft^2

$\rho_g = .026$ lb/ft^3

Solving Eq. 3.1-32 for G_f yields .022 lb/ft^2 sec

Solving Eq. 3.1-33 for G_{MB} yields 31.7 lb moles of H_2/hr ft^2

G_B is calculated to be 63.4 lb/ft^2 hr

Indeed it is evident that $G_{MB} >> 1 \frac{\text{lb mole}}{\text{hr ft}^2}$, therefore

$G_{MB} \approx G_{MT} \approx G_M \approx 31.7$ lb moles of H_2/hr ft^2. Referring to Eq. 8, a necessary consequence of the preceding statement is that

$P_B \approx P_T \approx P \approx 5$ atm.

One can now utilize Eq. 18 to calculate the height of the tower. Because of the constant pressure, c_e is merely taken to be a constant throughout the length of the column.

c_e is computed using Eq. 36 with P equal to 5 atm, and $H_{H_2} = 2.5 \times 10^5$ atm/mole fraction. $c_e = 7 \times 10^{-5}$ lb mole/ft^3. All constants in Eq. 18 are the same as those employed in the design of the O_2 tower except

$L = 23{,}000$ lb/hr ft^2

$c_B = 4.2 \times 10^{-5}$ lb mole/ft^3

$c_e = 7 \times 10^{-5}$ lb mole/ft^3

$D = 12 \times 10^{-5}$ ft^2 /hr

h comes out to be 3.2 ft.

Referring to Eq. 26, V = 3.2 ft^3

" " Eq. 28, $V_g = 2.18$ ft^3

" " Eq. 27, $t_g = 9 \times 10^{-4}$ hr

" " Eq. 30, $V_l = .33$ ft^3

" " Eq. 29, $t_l = 9 \times 10^{-4}$ hr

3.1.7 Summary of Design Parameters of the Towers

Parameter	O_2 Tower	H_2 Tower
P_B , (atm)	5	5
P_T , (atm)	5	5
c_B , (lb moles dissolved gas/ft^3 of solvent)	4.8×10^{-5}	4.2×10^{-5}
G_B , (lb gas/ft^2 hr)	540	63.4
G_T , (lb gas/ft^2 hr)	540	63.4
$G_{MB} \approx G_{MT}$ (lb moles gas/ft^2 hr)	16.9	31.7
$\overline{V}_B$, (ft^3 of gas/ft^2 hr)	1300	5350
$\overline{V}_T$, (ft^3 of gas/ft^2 hr)	1300	5350
$L_B \approx L_T$, (lb solvent/ft^2 hr)	10,200	23,000
$L_{MB} \approx L_{MT}$, (lb mole solvent/ft^2 hr)	482	1,100
$\overset{x}{V}_B \approx \overset{x}{V}_T$, (ft^3 of solvent)	138	313
h , (ft)	5.1	3.2
V , (ft^3)	5.1	3.2
V_g , (ft^3 of tower occupied by gas)	3.14	2.18
V_l , (ft^3 of tower occupied by liquid)	.33	.275
$t_g = t_l$, (hr)	2.4×10^{-3}	9×10^{-4}
$(c_B)(L_B)(1/\rho)$, (lb moles of gas absorbed/hr ft^2)	.0066	.0132

3.1.8 Pumping Requirements

As a crude approximation for the pumping requirements necessary, let the work performed by the pumps equal the mass transported times the differential height.

$$W = \left[(h)\ (L + G)\right]_{O_2} + \left[(h)\ (L + G)\right]_{H_2} \qquad 3.1\text{-}37$$

h_{O_2} = 5.1 ft

h_{H_2} = 3.2 ft

L_{O_2} = 10,200 lb/hr ft^2

L_{H_2} = 23,000 lb/hr ft^2

G_{O_2} = 540 lb/hr ft^2

G_{H_2} = 63 lb/hr ft^2

Therefore, W = 137,800 ft lb/hr = 5.15×10^{-2} $\frac{\text{kw hr}}{\text{hr}} = \frac{\text{52 watt hr}}{\text{hr}}$.

Our fuel cell produces 200 watts, so 26% of the power must be utilized for pumping. Based on the given assumptions, this system lies just on the borderline of feasibility. If different specifications were given, it is apparent that complete feasibility could be achieved for tower design. A full analysis requires combined treatment of a fuel cell model.

3.1.9 Nomenclature

a - theoretical interfacial area of packing, ft^2/ft^3

$\bar{a}$ - effective interfacial area of packing, ft^2/ft^3

A - cross-sectional area of the column, ft^2

B - used as a subscript refers to the bottom of the column.

c - concentration, lb/ft^3

D - diffusion coefficient of the gas in the solvent, cm^2/sec, ft^2/hr

e - used as a subscript refers to an equilibrium condition between the concentration of solvent and the gas above it.

f - used as a subscript refers to a flooding condition.

g - used as a subscript refers to the gas phase.

g - gravitational constant, ft/sec^2 , ft/hr^2

G - the mass flow rate of the gas, lb/hr ft^2 , lb/sec ft^2

h - height of the column, ft

H - Henry's Law constant, atm/mole fraction

i - used as a subscript refers to an interface

k - individual mass transfer coefficient, lb mole/hr ft^2 atm, lb mole/hr ft^2 lb mole ft^{-3}

K - overall mass transfer coefficient, lb mole/hr ft^2 atm, lb mole/hr ft^2 lb mole ft^{-3}

l - used as a subscript refers to the liquid phase

L - the mass flow rate of the liquid phase, lb/hr ft^2

M - used as a subscript refers to molar quantities

MW - the molecular weight, lb/lb mole

Δn - no. of moles absorbed in the column, moles

N - rate of mass transfer, lb mole/hr ft^2

P - pressure, atm

R - gas constant, ft^3 atm/^oR lb mole

Re - Reynolds number, dimensionless

Sc - Schmidt number, dimensionless

T - used as a subscript refers to the top of the column

T - temperature, ^oR

V - volume of the column, ft^3

$\overline{V}$ - volumetric flow rate of the gas phase, ft^3/ft^2hr

$\overset{x}{V}$ - volumetric flow rate of the liquid phase, ft^3/ft^2hr

W - power output of the pumps, ft lb/hr, kw, watts

w - used as subscript refers to water

X - mole fraction, dimensionless

ϵ - void volume coefficient, dimensionless

μ - viscosity of the liquid phase, centipoise, lb_M/ft hr

ρ - density of the liquid phase, lb/ft^3

References

(1) Perry's Chemical Engineers Handbook, 4th Edition, McGraw Hill Book Company, 1963, p. 14-15

(2) Van Krevelen and Hoftijer, P. J. Recveil des Trav. Chim. Pays Bas, 66, 49 (1947)

(3) Van Krevelen and Hoftijer, J. Chem. Eng. Progress, 44, 529 (1948)

(4) International Critical Tables

(5) Perry loc cit (ref 1) p. 3-77

(6) Perry loc cit pp. 18-28, 18-35

(7) Gubbins and Walker, Journal of the Electrochemical Society, 112, 469 (1965)

(8) Perry loc cit pp. 14-26

(9) Perry loc cit p. 14-5

(10) Sawistowski and Smith, Mass Transfer Process Calculations, Interscience Publishers (1963) p. 15-17

(11) Geffken, Z., Für Physikalische Chemie, 49, 268 (1904)

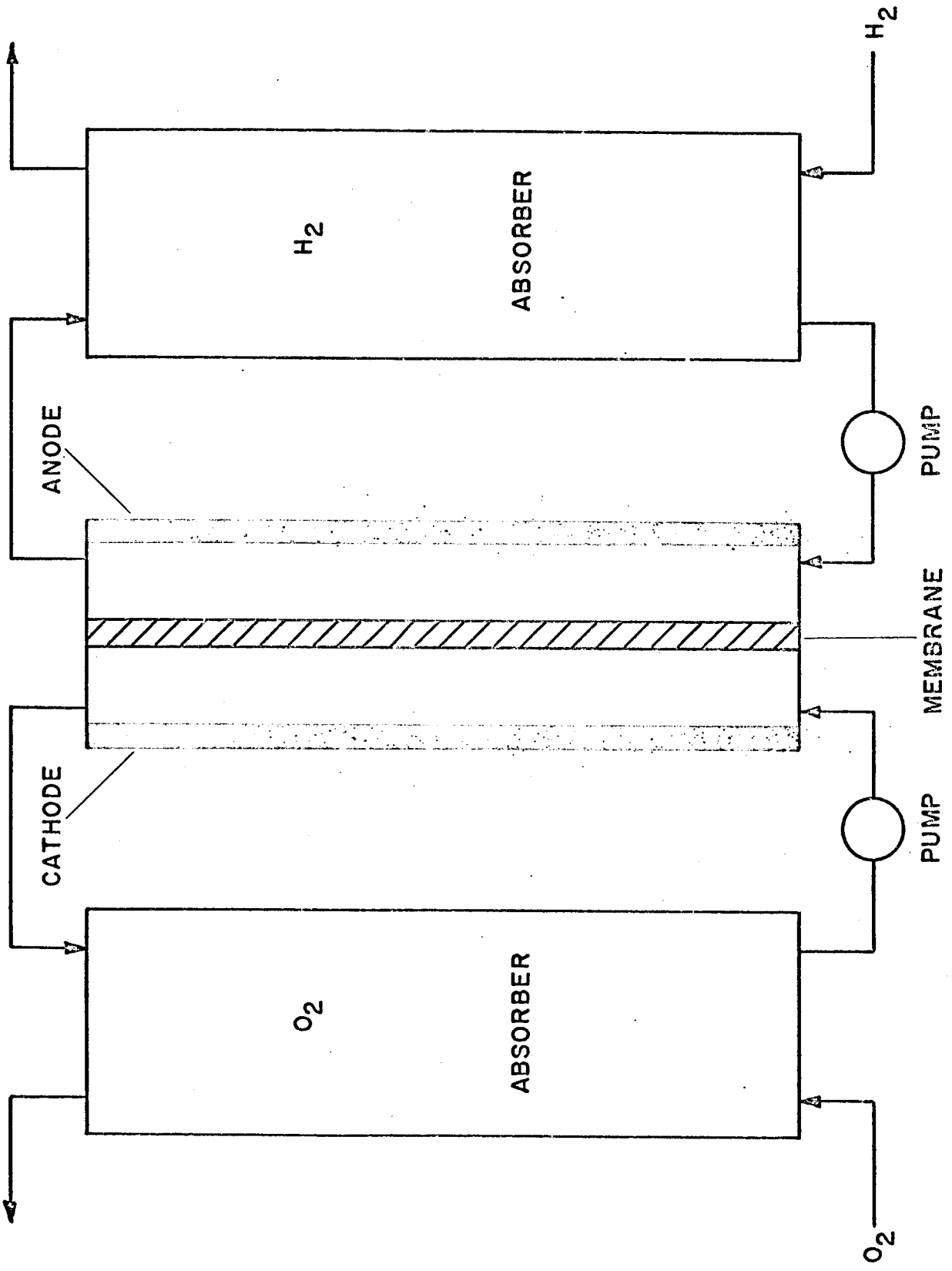
H_2
H_2 ABSORBER
ANODE
PUMP
MEMBRANE
CATHODE
PUMP
O_2 ABSORBER
O_2

FIG. .1-1

3 OVERPOTENTIAL-TIME VARIATION FOR GALVANOSTATIC CHARGING WITH POTENTIAL DEPENDENT CAPACITANCE 6

6 Leonard Nanis, Phillippe Javet 4

The non-linear differential equation for the time variation of overpotential during galvanostatic charging is solved by introducing a close approximation for the second term of rate equation. The results obtained are in close agreement with known solutions, covering all values of transfer coefficient, and are simple in form. Further, the incorporation of potential dependent capacitance is readily accomplished. Computations for such cases are shown to have a considerable effect on the overpotential transient.

A simple and useful relation describing the time variation of overpotential, η, following the switching on of a constant current density, J_T, has been determined. In the absence of mass transport effects (activation overpotential only), two separate reactions take place -

1. The normal Faradaic relation, involving current density J_F.
2. Charging of the double layer capacity, C, using current density J_C.

It is well-known that -

$$\frac{J_F}{J_o} = \exp\left(\frac{\alpha z F \eta}{RT}\right) - \exp\left(\frac{-(1-\alpha) z F \eta}{RT}\right) \qquad \text{Eqn. 3.4-1}$$

$$J_c = C \frac{d\eta}{dt} \quad \text{(per unit area)} \qquad \text{Eqn. 3.4-2}$$

$$J_T = J_F + J_c \qquad \text{Eqn. 3.4-3}$$

In general, the differential equation obtained from the above relations is non-linear and cannot be integrated. Two types of simplification can be made.

1. Let C be independent of potential. This has been done by some authors[1,2,3] who can ultimately obtain the relation between time and overpotential - but only for particular values of the coefficient of transfer α (i.e. $\alpha = 0$; $\alpha = 0.5$; $\alpha = 1$).

2. Approximate the value of J_F by one of the classical methods (linearization, Tafel). This has been done for the decay by Frumkin[4], but the application of Tafel relation for the charging transient has never been used, owing to the fact that this approximation does not pass through the origin of the η - J coordinate, which leads to very important errors at small times.

The present approach consists of modifying the Tafel equation in order to let it pass through the η - t origin. One obtains in this case -

$$J_T = J_o \exp\left(\frac{\alpha z F \eta}{RT}\right) - 1 + C \frac{d\eta}{dt} \qquad \text{Eqn. 3.4-4}$$

This relation can easily be integrated and has been compared to the analytic equations obtained by Karasyk[3] for some particular values of α. The agreement between the new approximation and the analytic solution has been found to be very satisfactory. The advantage of the present treatment is that Eqn. 4 can be integrated even if C is not a constant. The actual potential dependence of electrode-electrolyte interfacial capacitance has not been treated previously. For a linear dependence of capacitance with overpotential given as

$$C(\eta) = C_o + 2C_1 \eta \qquad \text{Eqn. 3.4-5}$$

the result is obtained as

$$t = \left(\frac{1}{J_T + J_o}\right)\left[C_o \eta + C_1 \eta^2 + \sum_{m=1}^{\infty} (-1)^m C_o \frac{I^m}{mb} e^{mb\eta} + \right.$$
$$+ \sum_{m=1}^{\infty} (-1)^m \frac{2C_1}{m^2} \frac{I^m}{b^2} (mb\eta - 1) e^{mb\eta} -$$
$$\left. - \sum_{m=1}^{\infty} (-1)^m I^m \left[\frac{C_o}{mb} - \frac{2C_1}{m^2 b^2}\right]\right] \qquad \text{Eqn. 3.4-6}$$

where $b = \alpha zF/RT$ and $I = J_o/J_o + J_T$.

The summation terms in Eqn. 6 are rapidly convergent and are readily applied to obtain the time-overpotential relation, since most of the terms are repetitive. Two hypothetical cases of capacitance variation have been treated:

Case 1: Capacitance increasing with overpotential

$$C(\eta) = 4.0 + 53.4\,\eta\ ,\ \mu F\ cm^{-2}$$

Case 2: Capacitance decreasing with overpotential

$$C(\eta) = 20.0 - 53.4\,\eta\ ,\ \mu F\ cm^{-2}$$

Case 3: $C = 12\ \mu F\ cm^{-2}$

Substitution of these relations in Eqn. 6 for $J_o = 10^{-3}\ Acm^{-2}$, $J_T = 0.1\ Acm^{-2}$, $\alpha = 0.5$, $z = 1$, $T = 300^{o}K$ leads to a steady state overpotential of 238 mV in all cases, but the transient is considerably different. At 20 microseconds, the overpotential has attained a value of 170 mV for Case 3, whereas Case 2 has reached only 126 mV. Case 1 at 20 microseconds has reached 205 mV and has reached steady state at 30 microseconds, while Case 2 and Case 1 converge after 30 microseconds and reach steady state well beyond 40 microseconds. The considerable curvature for Case 1 near the time origin suggests that care be exercised in the use of the initial slope of overpotential transients for the estimation of capacitance. These differences are readily seen in Figure .4-1.

References

1. W. A. Rojter, W. A. Juza, E. S. Polujan, Acta Physicochim. URSS, 10 3 389 (1939)

2. J. M. Matsen, J. Electrochem, Soc., 110 , 222 (1963)

3. L. Karasyk, R. W. Law, H. B. Linford, J. Electrochem. Soc., 111, 237 (1964)

4. A. Frumkin, Acta Physicochim. URSS, 18 , 23 (1943)

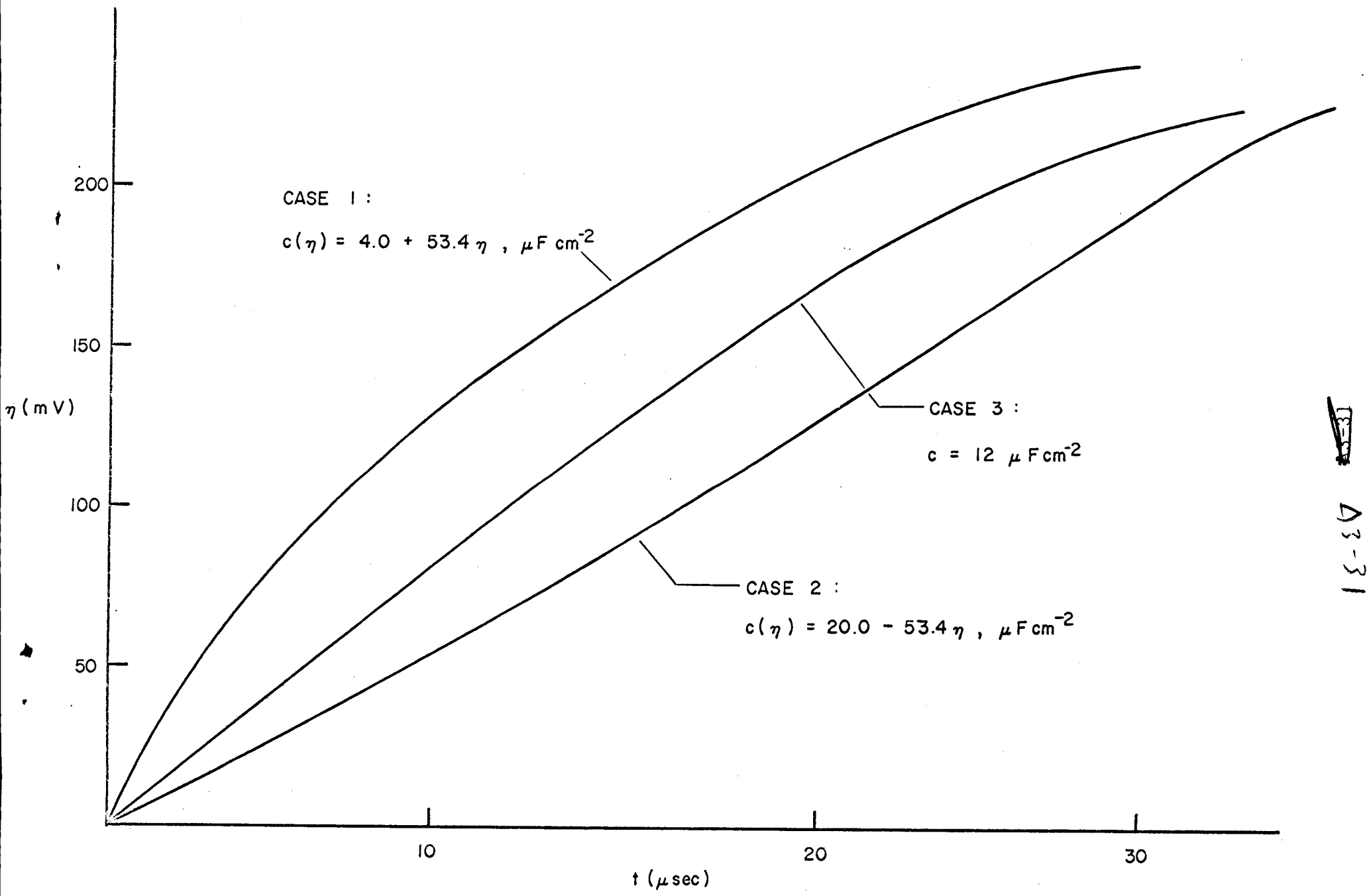
200
150
100
50
η (mV)
CASE 1 :
c(η) = 4.0 + 53.4 η , μF cm-2
CASE 3 :
c = 12 μF cm-2
CASE 2 :
c(η) = 20.0 - 53.4 η , μF cm-2
10
20
30
t (μsec)

D3-31

3 Current and Potential Distribution in Cylindrical Geometries: Engineering Applications to Fuel Cell Design 6

6 Leonard Nanis 8

In the design of fuel cells in which the electrolyte is "held" in a matrix or membrane, screens are generally used for electron collection. Such effort has been expended [2] in the performance of complex mathematical analyses which, in turn, usually require extensive machine computation of terms involving infinite series. Such an approach, while formally correct, is hardly conducive to ease of engineering application. In order to provide an alternative approach, use has been made of all the information to be gained from the solution of electrical field problems, especially the concept of partial resistance. Cylindrical geometry was chosen since screen contact impressions with a matrix are generally circular. The mathematical method used is based on transform methods and, as such, has been demonstrated to be utilitarian since the calculations have been checked as class and homework problems for the School of Chemical Engineering, Course 670, Electrochemical Engineering.

In the mathematical treatment of primary current distribution problems, it is generally necessary to evaluate the entire potential-space field as a solution to the Laplace equation

$$\nabla^2 \Phi = 0$$

Eqn. 3.3 - 1

At least three types of useful information for engineering application may be derived from the solution to Eqn. 3.3-1. First, the gradient of potential may be used to determine the variation of local current density, preferably in comparison with the average as $J/J_{ave.}$ Second, it is possible to assign an electrical resistance in the electrolyte to single electrodes. This type of result is useful in several applications such as electrolytic cell design and study of corrosion enhancement due to inclusions. The virtual resistance of electrolyte between two electrodes may be found by application of Ohm's law to the total potential difference between electrodes and the total current determined from the local current density integrated over the area of a particular electrode. It is generally true that potential varies rapidly with distance in the electrolyte in the immediate vicinity of an electrode, so that single electrode resistances are applicable. This prccedure may also be applied in the case of uniform current density over an electrode surface by use of the average potential of the electrode in question. Third, despite the usual mathematical complexity of the potential-space relation, effort should be directed at obtaining simplified limiting or special cases in order to evaluate the general extent of the potential field. For engineering purposes, this type of result is extremely useful since rules may be developed to permit the application of already obtained results to different electrode configurations. For example, the potential-space field for an isolated electrode may br examined to estimate the relative distances at which insulating tank walls do not affect the current distribution on the electrode.

The three above mentioned approaches have been applied to the example of a conducting disk located ($0 < r < a$; $z = 0$) at the bounding plane of a semi-infinite space filled with electrolyte ($z > 0$). Solution of Eqn. 1 in cylindrical coordinates

$$\frac{\partial^2 \phi}{\partial r^2} + \frac{1}{r}\frac{\partial \phi}{\partial r} + \frac{\partial^2 \phi}{\partial z^2} = 0 \qquad \text{Eqn. 3.3 - 2}$$

is facilitated by the use of Hankel (or Fourier-Bessel) transformation which converts Eqn. 2 in the transformed domain to

$$\frac{d^2 \bar{\phi}}{dz^2} - p^2 \bar{\phi} = 0 \qquad \text{Eqn. 3.3 - 3}$$

Eqn. 3 has a general solution

$$\bar{\phi} = A_1(p) e^{-pz} + A_2(p) e^{pz} \qquad \text{Eqn. 3.3 - 4}$$

where A_1 (p) and A_2 (p) are functional coefficients determined by the boundary conditions associated with Eqn. 2 . The boundary conditions are met after a simple inversion of Eqn. 4 back to the r , z domain as which for $A_2(p) = 0$ becomes

$$\phi(r,z) = \int_0^\infty p J_0(pr) A_1(p) e^{-pz} \, dp \qquad \text{Eqn. 3.3 - 5}$$

where J_0 is the Bessel function of first kind, zero order.

Case 1. Disk at Constant Potential

The boundary conditions for the disk at constant potential with the rest of the plane $z = 0$ as an insulator are

$$\phi = r_o \; ; \quad 0 < r < a \; , \; z = 0 \qquad \text{Eqn. 3.3 - 6}$$

$$\frac{\partial \phi}{\partial z} = 0 \; ; \quad a < r < \infty \; , \; z = 0 \qquad \text{Eqn. 3.3 - 7}$$

A counter electrode remote from the disk is characterized as

$$\phi = 0 \quad ; \quad z \to \infty \qquad \text{Eqn. 3.3 - 8}$$

The condition in Eqn. 8 permits the dropping of the positive exponential term in Eqn. 4

The use of particular Weber-Schafheitlin discontinuous integrals fitted to Eqn. leads to the result

$$V(r,z) = \int_0^\infty \frac{2V_o}{\pi} J_o(pr) \sin ap \; e^{-pz} \frac{dp}{p} \qquad \text{Eqn. 3.3 - 9}$$

which has an equivalent as

$$V(r,z) = \frac{2V_o}{\pi} \sin^{-1} \left\{ \frac{2}{\left[\left(\frac{r}{a} - 1 \right)^2 + \left(\frac{z}{a} \right)^2 \right]^{1/2} + \left[\left(\frac{r}{a} + 1 \right)^2 + \left(\frac{z}{a} \right)^2 \right]^{1/2}} \right\} \qquad \text{Eqn. 3.3 - 10}$$

The local current density is determined using Eqn. 9 in the relation

$$J = -K \frac{\partial V}{\partial z} \quad ; \; z = 0 \; , \; 0 < r < a \qquad \text{Eqn. 3.3 - 11}$$

(where = conductivity giving the result

$$J(r) = \frac{2KV_o}{\pi} \frac{1}{\sqrt{a^2 - r^2}} \qquad \text{Eqn. 3.3 - 12}$$

Eqn. 12 may be integrated to obtain J_{ave} , finally yielding

$$\frac{J(r)}{J_{ave}} = \frac{1}{2} \frac{1}{\sqrt{1-\left(\frac{r}{a}\right)^2}} \qquad \text{Eqn. 3.3 - 13}$$

This result shown in Eqn. 13 resembles in form that for a strip of width 2a imbedded in an insulating wall obtained by Wagner[1] using conformal mapping methods.

Eqn. 10 may be evaluated to indicate that the potential in the electrolyte has diminished to $V_o/10$ in a distance where $r/a \approx 6$ and $z/a \approx 6$.

By considering the average current density over the area of the disk, a total current of $4\,k\,V_o\,a$ is associated with an interelectrode potential difference of V_o , so that, from Ohm's law, the resistance associated with the disk is

$$R = \frac{1}{4Ka} \qquad \text{Eqn. 3.3 - 14}$$

Case 2. Constant Current Density on the Disk

A constant current density is specified by a condition of constant derivative of potential normal to the electrode as

$$\frac{\partial \phi}{\partial z} = -\frac{J}{K} \; ; \; 0<r<a \; , z=0 \qquad \text{Eqn. 3.3 - 15}$$

Together with the conditions specified by Eqn. 7 and 8, a result is obtained as

$$V(r,z) = \int_0^\infty \frac{Ja}{K} g_1(ap) g_0(pr) e^{-pz} \frac{dp}{p} \qquad \text{Eqn. 3.3 - 16}$$

In order to evaluate the current density along the disk, Eqn. 16 may be simplified for $z = 0$ to

$$V(r) = \frac{Ja}{K}\ {}_2F_1\left[-\tfrac{1}{2}, \tfrac{1}{2}; 1; \left(\tfrac{r}{a}\right)^2\right]; \quad 0<r<a, z=0 \qquad \text{Eqn. 3.3 - 17}$$

and

$$V(r) = \frac{Ja}{2K}\ \frac{a}{r}\ {}_2F_1\left[\tfrac{1}{2}, \tfrac{1}{2}; 2; \left(\tfrac{a}{r}\right)^2\right]; \quad a<r<\infty, z=0 \qquad \text{Eqn. 3.3 - 18}$$

where ${}_2F_1$ represents the hypergeometric function. In addition, a special solution to Eqn. 16 is available for $r = 0$ (center of disc) in order to evaluate the potential variation in the z direction. The result is

$$V(z) = \frac{Ja}{K}\left[\left(1+\left(\tfrac{z}{a}\right)^2\right)^{\frac{1}{2}} - \frac{z}{a}\right]; \quad r=0, \ z>0 \qquad \text{Eqn. 3.3 19}$$

From Eqn. 19, it may be seen that the potential at the center ($r = 0$, $z = 0$) is Ja/k and diminishes to 10% of this value in a distance where $z/a \approx 5$.

Evaluation of Eqn. may be accomplished in terms of complete elliptic integrals of the first and second kind and lead to a sidewise variation of potential in the $z = 0$ plane for $r > a$ which diminishes slowly, reaching 10% of the center value in a distance $r/a \approx 4.7$.

The potential along the disk is obtained from Eqn. 17 in an equivalent form as

$$V(r) = \frac{Ja}{K}\ \frac{2}{\pi}\ E\left(\tfrac{r}{a}\right)^2 \qquad \text{Eqn. 3.3 - 20}$$

where E is the complete elliptic integral of the second kind. The average potential along the disk ($0 < r < a$) may be obtained by series expansion of the elliptic integral and termwise integration or by other methods. The result is

$$V_{ave} = \frac{8Ja}{3\pi K}; \quad 0<r<a, \ z=0 \qquad \text{Eqn. 3.3 - 21}$$

The resistance assocaited with the disk under constant current conditions may be determined from Eqn. 21 and Ohm's law as

$$R = \frac{8}{3\pi^2 K a} \qquad \text{Eqn. 3.3 - 22}$$

When compared with the resistance result obtained for Case 1 with the disk at constant potential (Eqn. 14), it may be seen that constant current density condition leads to an associated resistance (Eqn. 22) which is 8% greater.

Applications

The internal resistance in solid electrolyte fuel cells of the type considered by Eisenberg may be rapidly estimated in a particularly simple form by assuming individual screen contacts over a circular area to be in a parallel circuit to describe the overall resistance. Limits of application are determined from the spatial variation of potential and Eqn. 14 and Eqn. 22 provide bounds for the occurrence of overpotential and its effect on current distribution.

Consider a matrix with area A, thickness t, contacted on both sides by screens with mesh spacing h and wire diameter d . The number of contact points will be A/h^2 and each point will have a partial resistance, r_i , of

$$\frac{1}{4\,K\,\,d/2} < r_i < \frac{8}{3\,\pi^2\,K\,\,d/2} \qquad \text{Eqn. 3.3 - 23}$$

Since the individual contact points on one side of the matrix sheet (conductivity K) are in parallel, the total resistance of the assemblage (both sides) is obtained from

$$R_{TOTAL} = \frac{2\,r_i\,\,h^2}{A} \qquad \text{Eqn. 3.3 - 24}$$

A useful comparison is made with the resistance of the matrix sheet incorporated between continuous plates, i.e., the theoretical resistance (which does not, of course, permit full gas access to the electrode-electrolyte interface). This theoretical resistance is simply

$$R_{Theoretical} = \frac{1}{K}\quad\frac{t}{A} \qquad \text{Eqn. 3.3 - 25}$$

Thus combining Eqn. 25 and 24 gives

$$\frac{R_{actual}}{R_{theo}} = \frac{2\,r_i\,\,h^2}{t}\quad K \qquad \text{Eqn. 3.3 - 26}$$

For an assumed constant potential contact,

$$\frac{R_{actual}}{R_{theo}} = \frac{h}{t}\quad\frac{h}{d} \qquad \text{Eqn. 3.3 - 27}$$

From the field extent considered above Eqn. 10, Eqn. 27 may be used provided

$$\frac{h}{d} \geq 6 \text{ and } \frac{t}{d} \geq 6 \text{ or thus } \frac{t}{h} > 1.$$

For the case of uniform current distribution over the contact area,

$$\frac{R_{actual}}{R_{theo}} = 1.08 \frac{h}{t} \frac{h}{d} \qquad \text{Eqn. 3.3 - 28}$$

Similar space limits as for Eqn. 27 are appropriate. It seems reasonable, based on throwing power considerations, that Eqn. 28 is more realistic than Eqn. 27. The utility of these results (Eqn. 27, 28) is best seen by comparing resistance ratios reported by Eisenberg[2] based on extensive termwise machine computation of a very complex result. For $d/h = 0.1$, $h/t=1$, the analytic solution has been evaluated to give a resistance ratio of 10.97 whereas from Eqn. 27 and 28

$$10 < \frac{R_{act}}{R_{theo}} < 10.8$$

In another example, for $d/h = 0.5$, $h/t = 1$, present results indicate

$$2 < \frac{R_{act}}{R_{theo}} < 2.16$$

whereas the 100 term summation[2] yields a resistance ratio of 2.033. The work reported by Eisenberg[2] is based on constant potential considerations so that actually the present approach differs by only a few percent even when the $h/d > 6$ requirement is lowered to $h/d = 2$.

References

1. C. Wagner, J. Electrochem. Soc., 98 (1951) p. 116.
2. M. Eisenberg, "Advances in Electrochemistry and Electrochemical Engineering", Vol. 2, C. Tobias, editor, Interscience, p. 258.

3 Foaming Electrolyte Fuel Cell 6

Senior Investigator 6 Dr. L. Nanis

Research Specialist: Mr. A. Saunders 8

On considering the fundamental behavior of the fuel cell porous electrode as based on research and development in the past several years, it is clear that fuel gas diffusion plus the resistance of the thin electrolyte film must represent limiting factors on performance. In an attempt to depart from the concept of the conventional porous electrode, a system was visualized in which solution of fuel gas into the electrolyte can be accomplished from a foam structure. Such a foam, supported by the reactant gases, will ideally consist of masses of small bubbles with a wall thickness approaching 10^{-6} cm and will allow rapid diffusion of the trapped gas into the surrounding electrolyte film. The electrolyte in the foam will drain back to the main body of electrolyte via the electrode, thus providing a continuous supply of gas-saturated electrolyte to the working electrode surface.

By itself, concentrated KOH will not produce a foam when bubble stirred, so a suitable foaming additive must be found. This preliminary study has been made to evaluate the following four foaming agents which were readily available

(a) Sodium Oleate,

(b) GAFAC LO 529 (trade designation, General Analine and Film Co.)

(c) GAFAC PE 510 "

(d) GAFAC RE 610 "

The requirements are that the foamant must operate in an alkaline electrolyte without degradation or chemical reaction. The cell, shown schematically in Figure 3.2-1, did not adequately prevent the electrolyte from passing through the frit under the impetus of the bubbling gas. Thus a degree of electrode depolarization was present at all times. Current

measurements represent the steady state following a decay from higher values produced by load changes. The electrodes were 1 cm x 0.5 cm x 0.025 cm Pt. sheet which were cleaned with 1 : 1 Aqua Regia, well washed in distilled water and then 6N KOH before being admitted to the cell. The cell electrolyte was 6N KOH.

Of the four foaming agents tested, (a) and (b) were found to be unsuitable owing to a rapid drop in open circuit voltage. (c) initially appeared suitable, but, here again, after being used for several hours, open circuit voltages were found to be dropping. (This may not be due to the foamant but to other impurities and needs to be examined again.) Of the four tested, (d) was undoubtedly the best as is shown in Figure 3.2-2.

In Figure 3.2-2 the cell current and potential are shown for 6N KOH with smooth platinum electrodes. Where the platinum electrodes were fully immersed below the solution level, a gentle stirring was provided by hydrogen and oxygen flow in the respective compartments. The gas flow rate was 2-3 cc per minute and the cell resistance, measured with an a.c. bridge, was minimal, i.e., 8 ohm. Some improvement of the current-voltage curve was obtained by flowing gas in each compartment at a rapid rate (100 cc per min.) so as to completely disturb the liquid surface. The enhanced mass transport resulted in greater cell potentials for a given current in comparison with full immersion and gentle stirring. The cell resistance was 25 ohm with the electrodes in the violently agitated electrolyte "surface" region. A limiting current density was detected.

The uppermost line in Figure 3.2-2 represents 6N KOH with the addition of GAFAC RE 610 foamant at a concentration of 1 gm per liter. The platinum electrodes were lifted clear of the electrolyte surface so that 5 mm of separation between the electrolyte and the bottom edge of the vertical sheet electrode existed. The cell resistance increased to 380 ohm.

Despite the increase in cell resistance because of the lengthened electrolyte path in the foam the output of the cell was markedly improved. It should be noted that the flow rate for fuel gas was small (2-3 cc/min). Proper comparison of this result is best made with the most nearly vertical curve in Figure 3.2-2 (immersed electrodes). Although foam raises the cell resistance between electrodes from 8 ohm (electrodes immersed) to 380 ohm (electrodes in foam region), the current-voltage response is greatly improved. It is concluded that foam electrolyte is a workable alternative to the porous electrode. Further work will entail patent application, engineering of designs to optimize power output, and study of further foaming agents both as to nature and optimal concentration. It seems reasonable that a very stable foam is not quite as desirable as one which soaks up hydrogen (and oxygen) in the large area - small diffusion path liquid boundary of the bubble network and then breaks structure, causing the fuel rich electrolyte to run down along the electrode surface.

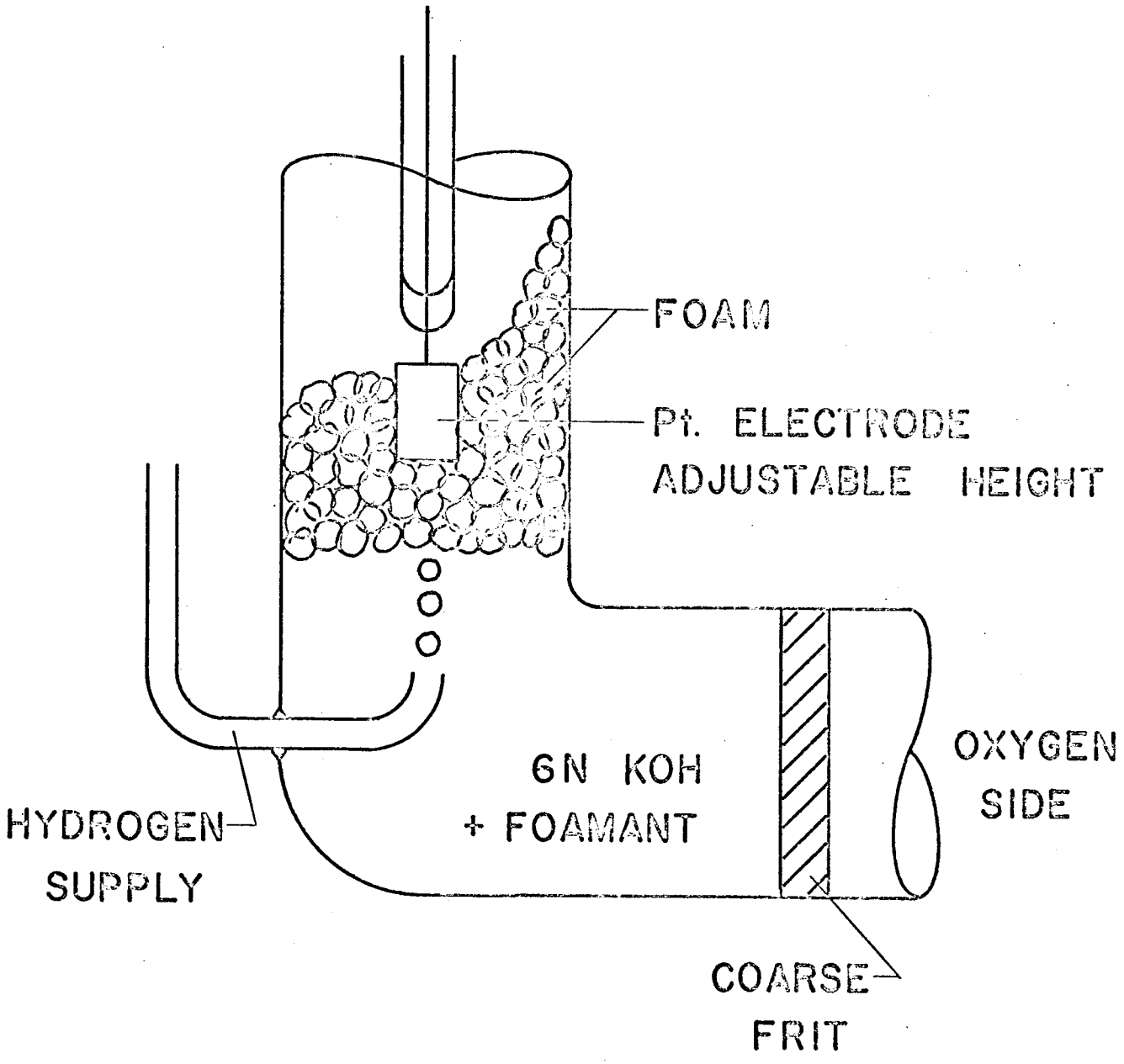
FOAM
Pt. ELECTRODE
ADJUSTABLE HEIGHT
6N KOH
+ FOAMANT
HYDROGEN
SUPPLY
OXYGEN
SIDE
COARSE
FRIT

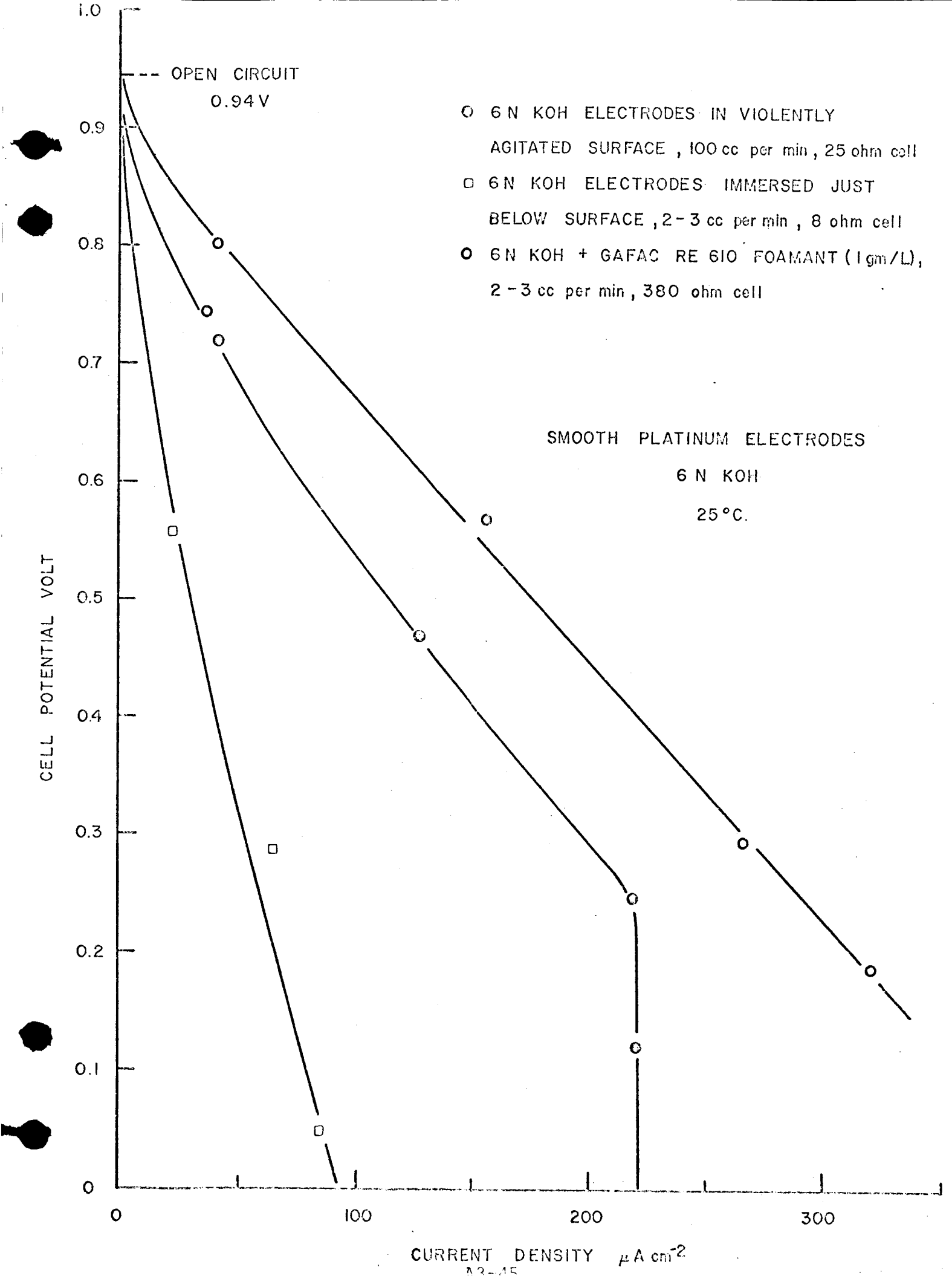
OPEN CIRCUIT
0.94 V
O 6 N KOH ELECTRODES IN VIOLENTLY AGITATED SURFACE, 100 cc per min, 25 ohm cell
□ 6 N KOH ELECTRODES IMMERSED JUST BELOW SURFACE, 2-3 cc per min, 8 ohm cell
O 6 N KOH + GAFAC RE 610 FOAMANT (1 gm/L), 2-3 cc per min, 380 ohm cell
SMOOTH PLATINUM ELECTRODES
6 N KOH
25°C.
CELL POTENTIAL VOLT
1.0
0.9
0.8
0.7
0.6
0.5
0.4
0.3
0.2
0.1
0
0
100
200
300
CURRENT DENSITY μA cm⁻²